CONCERT-Japan
Research and Innovation Joint Call

Efficient Energy Storage and Distribution
Resilience against Disasters

RAPSODI Project

Risk Assessment and design of Prevention Structures
fOr enhanced tsunami DIsaster resilience

Deliverable D8 – A GIS tsunami vulnerability and risk assessment model
2nd year of funding

20120768-08-R
30 June 2015
Revision: 0

CONCERT JAPAN
Connecting and Coordinating
European Research and Technology Development with Japan
www.concertjapan.eu

This work was supported by funding received from the CONCERT–Japan Joint Call on Efficient Energy Storage and Distribution/Resilience against Disasters

Project information

Name of the project:	RAPSODI
Start of the project:	01 July 2013
Duration (no. of months):	24
End of the project	30 June 2015
Name and country/region of each partner	NGI, Norway; PARI, Japan; TU-BS, Germany; METU, Turkey
Overall budget	383 k€

Client

Client:	CONCERT-Japan Joint Call Secretariat
Client's contact persons:	CONCERT-Japan Coordinator The Scientific and Technological Research Council of Turkey (TUBITAK) Ms. Filiz Hayirli (filiz.hayirli@tubitak.gov.tr) concertjapan@tubitak.gov.tr Phone: + 90 312 468 5300 (ext.1910) CONCERT-Japan Joint Call Secretariat Centre national de la recherche scientifique (CNRS) Ms. Lucie Durocher (lucie.durocher@cnrs-dir.fr) Phone: + 33 (0)1 44 96 47 14 Fax: + 33 (0)1 44 96 48 56 http://www.concertjapan.eu
Contract reference:	NGI 229578/H20; METU 113M556; TUBS 01DR13016
Settlement numbers:	PARI 2013 H25国際第1-33号 2014 H26国際第1-17号

For NGI

Project manager:	C.B. Harbitz
Prepared by:	R. Frauenfelder, C.B. Harbitz, S. Glimsdal, K. Sverdrup-Thygeson, J. Johansson, G. Kaiser
Reviewed by:	G. Kaiser, C.B. Harbitz, R. Frauenfelder

CONCERT JAPAN
Connecting and Coordinating European Research and Technology Development with Japan

Publishable summary

The 2011 Tōhoku tsunami clearly showed the potential for massive destruction of buildings, infrastructure, and coastal protection by tsunamis. A huge amount of data has been collected during and after the event, allowing retrospective analyses. The CONCERT-Japan RAPSODI (Risk Assessment and Design of Prevention Structures fOr enhanced tsunami Disaster resilience) project (http://www.ngi.no/en/Project-pages/RAPSODI/) is a project coordinated by NGI (Norway) with the partnership of PARI (Japan), TU Braunschweig (Germany), and METU (Turkey) aiming to use these data to develop a framework for quantitative tsunami risk analysis and to design tsunami mitigation structures to improve resilience against tsunami impacts. The methods developed within the framework of the project are based on the results and findings from three project stages, including: (i) evaluation of existing knowledge and comparison of mitigation strategies, (ii) numerical and experimental studies, and (iii) tsunami vulnerability assessment and risk management.

The tsunami mortality risk-analysis model is based on very high-resolution (VHR) digital surface elevation data, numerical modelling of tsunami inundation, building type/vulnerability and population data, and empirical relations for damage and fatalities as a function of tsunami flow depth. For further validation and development, the model has been used in the RAPSODI project for hindcasting the 2011 Tōhoku tsunami in two locations: Sendai and Ishinomaki.

The inundation modelling is performed with digital elevation models of various resolution and quality. SRTM-based inundation modelling consequently overestimates the inundation distance, while the ASTER based inundation modelling clearly underestimates the inundation distance. The inundation modelling based on the VHR Japanese digital elevation model is also overestimating the inundation distances, but to a less extent than the SRTM-based modelling. The results of the VHR-based inundation modelling agrees favourably with the observations of inundated areas and flow depth (water marks). It should be noted that buildings and infrastructure were not included in the simulations. Such obstructions will normally increase the flow resistance and thus reduce the inundation distance.

As building vulnerability was not available to us in an appropriate format, a synthetic uniform building vulnerability was introduced for the built-up areas within the Ishinomaki city boundaries. To evaluate the human population exposure to the tsunami, the population census data for 2010 were used. With reasonable choices of building vulnerability, the estimated expected number of fatalities for Ishinomaki city agree well with the reported death toll. Accessing the large amount of potentially available post-disaster field data was more challenging than expected when carrying out the tsunami mortality risk modelling in the RAPSODI project.

The results of the mortality hindcast for the 2011 Tōhoku tsunami substantiate that the GIS tsunami risk model can help to identify high mortality risk areas, as well as identify the main risk driver(s) in high-risk areas, which often can be attributed to high to very high flow depths, high population concentrations and/or vulnerable population mixture (resulting in high exposure), vulnerable building mass, or a combination of these factors. The model can further be used e.g. to produce maps showing different mortality risk scenarios to be expected for different flow depth scenarios with corresponding probabilities. This could help in meaningful urban planning, allowing for the identification and selection of evacuation routes, shelter locations, planning of mitigation structures, etc.

The design of the GIS-based tsunami mortality risk model allows for expansion of the model with new or other parameters, as well as for the refinement of already implemented parameters.

Contents

1 Introduction

During recent years, NGI has developed a generic GIS-based model for local analyses of tsunami mortality risk (i.e. loss estimates; NGI 2009a, 2009b). The model was initially developed for a (hypothetical) tsunami forecast scenario affecting the town of Bridgetown, Barbados in the Caribbean (2009c) and further developed in a forecast study in the Philippines, for the city of Batangas (2009d). The model was later successfully tested by hindcasting the 2009 South Pacific tsunami in American Samoa (Harbitz et al., 2011).

For further validation and development, the model has here been used in the RAPSODI project for hindcasting the 2011 Tōhoku tsunami in two locations: Sendai and Ishinomaki.

Detailed surveys of tsunami vulnerability models and previous analysis of tsunami hazard and risk are presented by González-Riancho (2014a, 2014b) and in RAPSODI Deliverable 1 "Existing tools, data, and literature on tsunami impact, loads on structures, failure modes and vulnerability assessment" (METU 2015).

2 Background of the 2011 Tōhoku earthquake and tsunami

The magnitude (Mw) 9.0 Great East Japan earthquake occurred at 14:46 (Japanese Standard Time) on March 11th 2011. The earthquake mechanism was reverse faulting at a depth of 24 km on the subduction zone plate interface at the Japan Trench, with the epicentre at N38.1, E142.9, 130 km offshore of the Oshika Peninsula (Japanese Meteorological Agency, 2011).

The total rupture area is estimated to be 380 km long and 90-130 km wide (Geospatial Information Authority of Japan, 2011). Strong ground shaking was felt across Japan, and while the Japanese Meteorological Agency (JMA) shaking intensity 7 was recorded at one location (Kurihara City, Miyagi Prefecture), locations in Iwate and Miyagi Prefectures generally experienced maximum JMA intensities of 5 Lower to 6 Upper. This level of shaking corresponds approximately to Modified Mercalli Intensities 7 to 10, used in New Zealand and the U.S. (Fraser et al., 2012).

Seafloor geodetic data indicate co-seismic displacement of up to 3 m in an upward direction (Sato et al., 2011), which was sufficient displacement to generate the tsunami that caused damage along the entire east coast of Honshu, and particularly significant damage in Iwate, Miyagi, Fukushima, and Ibaraki Prefectures. Coastal towns were afforded a minimum of around 20-25 minutes between the earthquake and the arrival of the first significant (inundating) tsunami. Some areas, such as Ishinomaki City, experienced five significant waves, the latest of these arriving at least 2 hours and 15 minutes after the earthquake. Many areas (for example, Natori City and Kesennuma City) remained inundated with standing water until at least March 12th 2011, with frequent subsequent flooding due to co-seismic subsidence at

the coast of up to 1.2 m (Geospatial Information Authority of Japan (GSI), 2011). In Kesennuma, fires that had ignited during the initial tsunami waves continued to burn on March 12th. (Fraser et al., 2012).

The Tōhoku tsunami caused severe damages to buildings and infrastructure along the 2000 km coastline affected. Tsunami impacts varied according to local conditions. The first wave was not always the largest one, and huge differences in tsunami run-up and inundation extent occurred between the Sendai plains and the northern Sanriku coast. While the inundation extent was much larger in the floodplains of Sendai, run-up is considerably higher along the Sanriku coast. Moreover urban areas, coastal structures, geomorphology, and rivers influenced the inundation patterns (Mori et al. 2011). Along rivers the inundation distance was longer and water has been transported far into the hinterland. Due to locally varying hazard conditions, but also due to local factors determining vulnerabilities, including population density, coastal protection measures, building material or early warning capacities, impacts and damages were different at different locations. In the aftermath of the event several survey teams mapped and quantified fatalities and damages in the affected areas (e.g. EERI 2011; Vervaeck and Daniell, 2011; Goto et al., 2011). One of the most comprehensive overview reports concerning the first surveys was published by Takahashi et al. (2011) on April 28, 2011. A later important report presented by Ranghieri and Ishiwatari (2014) summarizes the lessons learned from the Great East Japan Earthquake and Tsunami and provides guidance to other disaster-prone countries for mainstreaming Disaster Risk Management (DRM) in their development policies. A more comprehensive overview is also presented by NGI (2011). Main results are summarized as follows:

- In total 20 000 people were recorded dead or missing, and 400 000 people were homeless (Vervaeck and Daniell, 2011; EERI, 2011; Dunbar et al., 2011). Most fatalities occurred in the prefectures Iwate (4664/1628 missing), Miyagi (9487/2092 missing), and Fukushima (1604/238 missing) (Dunbar et al., 2011; Figure 2.1).
- Shortly after the event, the costs of the damages summed up to an order of magnitude of $300 billion in direct losses (EM-DAT, 2011; Mimura et al,. 2011; Mori et al., 2011). An extraordinarily high number of indirect losses in terms of reduced economic activity and interruption of supply chains for a longer period was also expected. After all, damages are estimated to be the highest economical loss from an earthquake/tsunami ever (Vervaeck and Daniell, 2011; EERI, 2011). The structural damages, especially those to buildings, were particularly high, which is supposed to be due to the fact that most buildings in the area were wooden and only some major buildings were of concrete material. Although building regulations are very strict in Japan due to the extraordinary exposure to natural hazards, buildings in the area are mainly constructed to withstand earthquakes. This resulted in very little damage to buildings caused by the earthquake but major damages caused by the tsunami, since wooden, earthquake resistant houses are not well fitted to withstand a tsunami. For the first 3 km

inland, however, most of the buildings have been destroyed, regardless of their structure (Gomez et al., 2011).

- Besides buildings, also port facilities and related constructions were severely damaged (e.g. in Ishinomaki). Quay walls and piers were widely destroyed by the waves or the impact of objects such as boats and containers.
- Besides the loss of life and the material damage, environmental impacts occurred. The most significant environmental impact is of course related to the leak of nuclear radiation from the Fukushima power plant. Another environmental impact related to the tsunami is the pollution by waste and debris. In agricultural areas land was inundated and salt water intrusion is going to affect future cropping (e.g. in Rikuzentakata, over 70% of the land was affected by salinization; EERI, 2011). The earthquake triggered also secondary environmental impacts, such as e.g. 200 landslides (Vervaeck and Daniell, 2011).

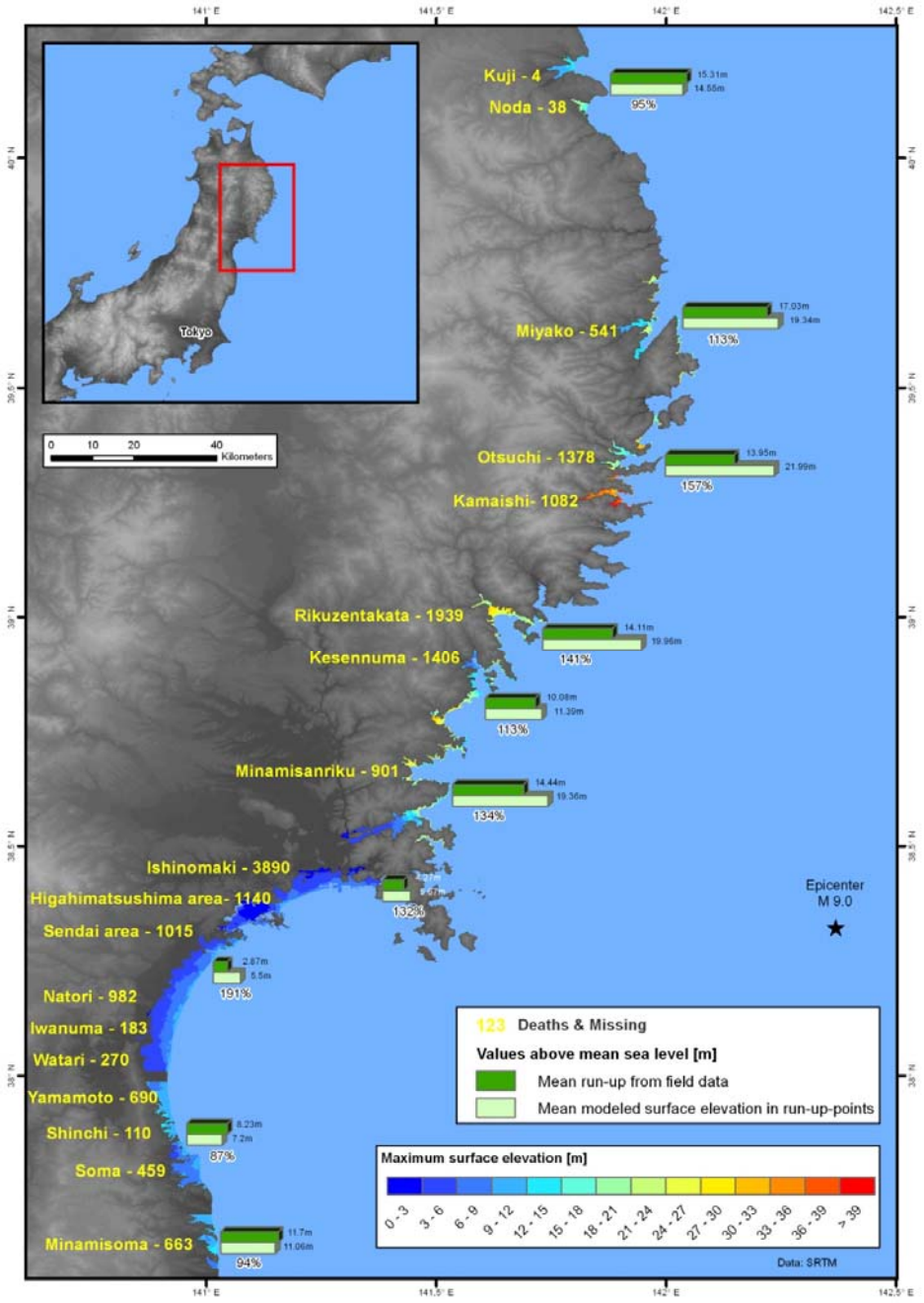

Figure 2.1: Number of fatalities by community (based on EERI, 2011) combined with mean measured and modelled run up (scenario D dispersive) (from NGI, 2011; modified from Løvholt et al., 2012).

3 Tsunami hazard and risk mapping

3.1 General aspects of tsunami hazard and risk mapping

Tsunami hazard maps show the inundation extent of various scenarios with corresponding probabilities (alternatively, they show the probabilities for a given threshold run-up height). Risk maps go a step further by considering also the consequences for the elements at risk. The maps are meant for land use planning, comparison with other threats, warning and handling acute situations, etc. The contents, scale, and detailing level of maps for natural hazard and risk assessment should be adapted to the intended use and the available input data. For instance:

- A *regional tsunami exposure assessment* may combine calculated maximum water levels at the shore line for given scenarios and probabilities with simplified inundation estimates and population densities.
- A *local tsunami risk assessment* may include more sophisticated simulations of the inundation for the given scenarios and probabilities in combination with the elements at risk (people, economic and/or ecological values, etc.) and their vulnerability (mortality, building vulnerability, etc.).

The scale and contents of the maps can vary over the whole range from "global" to "local", depending on the intended use. Typically, maps for land use planning, handling of acute hazard situations, or various kinds of risk assessment in local communities can be presented at a scale larger than 1 : 5000 (often preferable with a scale equal to or even larger than 1 : 2500). Different scales for different users should be considered.

Contents of maps intended for land use planning with regard to tsunamis (for a given probability) are typically:

- Hazard maps: Inundation distance and inundation height (or flow depth) for various scenarios
- Wave speed or momentum (for currents) and momentum flux (for design loads), (wave energy will give a combined impression of elevation and momentum flux).
- Previous events (geological and historical records)
- Highly populated / vulnerable areas
- Exposure maps (distribution of population, distribution of values)
- Vulnerability maps
- Risk maps, risk zoning

Correspondingly, contents of maps for warning and handling of an acute tsunami situation (with a given probability or intensity) are typically:

- Inundated areas to be evacuated
- Highly populated / vulnerable areas

- Escape routes
- Elevated / safe areas
- Personnel to be warned

3.2 Methodology for creating risk maps

Important within the framework of the presented GIS-study is the calculation of the risk parameter and its input variables. These input variables are defined following the International Strategy for Disaster Reduction of the United Nations UN/ISDR (http://www.unisdr.org/). These ISDR definitions are, in the following, given in quotation marks with some additional information.

- Risk: "The probability of harmful consequences, or expected losses (deaths, injuries, property, livelihoods, economic activity disrupted or environment damaged) resulting from interactions between natural or human-induced hazards and vulnerable conditions. Conventionally risk is expressed by the notation Risk = Hazards x Vulnerability." Risk can be expressed as probable loss calculated as an average annual value or for a particular scenario.
- Hazard: "A potentially damaging physical event, phenomenon or human activity that may cause the loss of life or injury, property damage, social and economic disruption or environmental degradation". Each hazard is characterized by its location, intensity, and probability.
- Exposure: "People, property, systems, or other elements present in hazard zones that are thereby subject to potential losses".
- Vulnerability: "The conditions determined by physical, social, economic, and environmental factors or processes, which increase the susceptibility of a community to the impact of hazards", i.e. the possibility of an element at risk (a person, a village, livelihood) to be damaged or destroyed by a hazard.

In this study, we calculate tsunami mortality risk using the following equations:

$$mortality\ risk = hazard * consequence \quad (1)$$

where

$$consequence = exposure * mortality \quad (2)$$

Inundation depth for the 2011 Tōhoku tsunami, called 'flow depth' hereafter, is obtained from a numerical simulation (Section 5; Løvholt et al., 2012) and is used to represent the *hazard*. In such a hindcast analysis performed primarily for model validation, not much attention is paid to the probability of the scenario; admittedly violating the definition of 'hazard'. The *consequence* is represented by the exposure and the mortality.

4 Basic GIS concepts of the tsunami mortality risk analysis model

The present study was carried out using the spatial analysis capabilities of a Geographic Information Systems (GIS). We used ArcMap (© by ESRI), but basically, the presented procedures can be effectuated with every standard GIS-software.

The data format best suited for the presented analyses are raster datasets (cf. Figure 4.1). A raster is a representation of the world as a matrix of equally sized cells. Each cell has a value (a number), and this value can represent some property or characteristic of the cell. In this case the value can be e.g. a population density, a building vulnerability score, or a flow depth. Cell size is the same within one raster, and ideally the same for all rasters and is chosen in accordance with the desired level of detail of the investigation to be carried out. Often, cell size is also determined by the resolution of the available input data. In the present GIS study we applied a cell size of 23 m x 23 m (i.e. 529 m^2 per cell), resampled from the selected resolution of the flow depth calculation (see section 4.1).

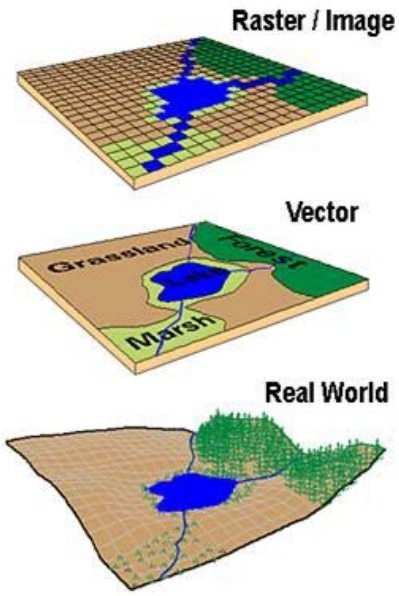

Figure 4.1: Representation of the real world and showing differences in how a vector and a raster GIS will represent this real world. The two primary spatial data encoding techniques in GIS are vector and raster. Source: http://campusarch.msu.edu (last access date: April 29, 2015).

4.1 Input data and main derivatives

The most important dataset for the inundation modelling is the digital elevation model (DEM). For our study areas, there exist DEMs for both the pre- and post-tsunami situations. Ideally, one would use the pre-tsunami topography for the modelling, accounting for the terrain at the time the tsunami hit the land.

Unfortunately, the pre-tsunami DEM data do not cover the entire area that was inundated. Therefore, we had to use post-tsunami DEM data for the inundation modelling. This is not ideal, but we assume that these data are still closer to the real original topography than the formerly available DEMs from the Shuttle Radar Topography Mission (SRTM, http://www2.jpl.nasa.gov/srtm/) or the ASTER Global Digital Elevation Map (http://asterweb.jpl.nasa.gov/gdem.asp). It should also be mentioned that the earthquake shifted the city of Ishinomaki southeast and downward, lowering it by as much as 1.2 metres (3.9 ft) in some areas, which supports the use of the post-tsunami (here rather interpreted as post-earthquake) DEM.

For the modelling runs presented here, the very high-resolution (VHR) DEM data from Geographical Survey Institute of MLIT, Japan, were resampled to 22.2 m x 17.5 m in order to reduce computing time, respectively in order to be able to run sufficiently large areas. However, it is of course possible to run the models for smaller areas with much higher resolution, since the original raster resolution is 0.0000617 deg x 0.0000617 deg in lat/long for Miyagiken and 0.0000206 deg x 0.0000206 deg for Ishinomaki and Rikuzentaka. Table 4.1 gives an overview of the basic input data and their main derivatives used in this study.

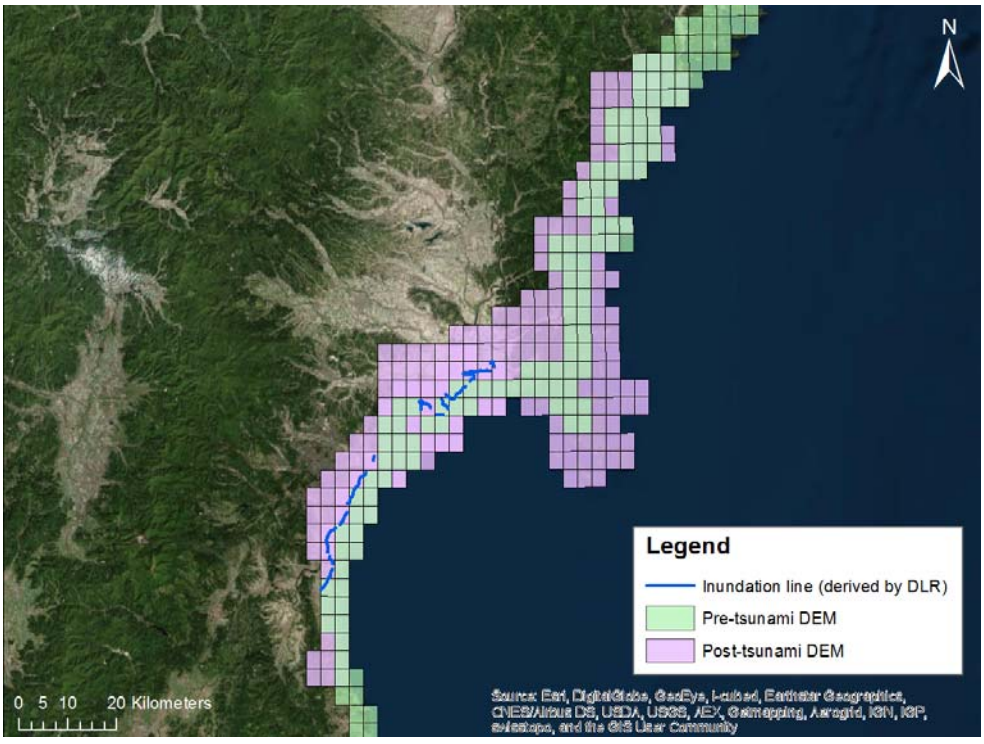

Figure 4.2: Miyagi Prefecture. Green rectangles = areas where pre-tsunami DEMs are available, purple = areas where post-tsunami DEMs are available; blue line = inundation line derived from satellite imagery by DLR (German Aerospace Center).

Table 4.1: Description and origin of the data which were used as input variables for the GIS-calculations. Note: name of datasets are, hereafter, given in sans-serif font.

Dataset	Datatype	Description	Origin
Pre_dem	Raster	Digital surface elevation model, original resolution 0.0000206 x 0.0000206 deg. Covering only part of the focus sites, hence not used.	Geographical Survey Institute of MLIT, Japan
Post_dem	Raster	Digital surface elevation model, original resolution 0.0000206 x 0.0000206 deg, respectively 0.0000617 x 0.0000617 deg.	Geographical Survey Institute of MLIT, Japan
Flow_depth	Raster	Ishinomaki: - FD_scenario D_v13_ Post_dem Sendai: - FD_scenario D_v13_ASTER DEM - FD_scenario D_v13_SRTM_DEM - FD_scenario D_v13_ Post_dem	Løvholt et al., 2012
• City_line • Building_outline • Building_area	Line Polygon Polgyon	City borders for Ishinomaki and Sendai Building outlines and overbuilt area for parts of Ishinomaki and Sendai	Data from the Geospatial Information Authority of Japan
Water mark	Point	浸水深 (immersion depth) Post-tsunami field measurements of flow depth	From "Reconstruction assistance research archive" http://fukkou.csis.u-tokyo.ac.jp/
Inundation area	Polygon	Inundated area	From "Reconstruction assistance research archive" http://fukkou.csis.u-tokyo.ac.jp/
Building disaster area	Polygon	エリア区分 (building damage)	From "Reconstruction assistance research archive" http://fukkou.csis.u-tokyo.ac.jp/
Building damage	Map	Map showing severeness of building damage (high, low, no damage) on individual building level	From WorldMap/Center for Geographic Analysis at Harvard University (http://worldmap.harvard.edu/japanmap/)
Mesh05741_census	Polygon	Population data (total population, no. of households, no. of females, no. of males)	Data by courtesy of Prof. Y. Maruyama, Department of Urban Environment Systems, Graduate School of

			Engineering, Chiba University, Japan.
Vuln_uniform	Polygon	Assumed mean structural building vulnerability	Since spatially located building vulnerability data were unavailable to us until shortly before project end, a mean vulnerability of 0.5 was assigned to the entire municipal area of Ishinomaki
Disaster extent	Map (jpg)	Sendai disaster extent map based on satellite imagery	http://www.un-spider.org/japan-pacific
Change detection	Map (jpg)	Sendai change detection map based on TerraSAR-X satellite imagery	http://www.un-spider.org/japan-pacific
Inundation overview	Map (jpg)	Sendai inundation overview map based on TerraSAR-X satellite imagery	http://www.un-spider.org/japan-pacific
Tsunami affected land	Polygon	Tsunami affected land area, Sendai	Unosat
Inundation line	Line	Inundation line for Sendai and Ishinomaki derived from satellite imagery from DLR	DLR
Inundation flow mask	Polygon	Flood mask derived from TerraSAR-X satellite imagery	DLR

4.2 Influence of DEM resolution and quality

Obviously, real topography and surface roughness have an important influence on the inundation pattern and the flow depth. Since DEMs are always only digital representations of the "true" world, their resolution, accuracy, and precision exert important boundary conditions on the model results. Figure 4.4 shows the comparison between the inundation modelling as carried out based on the SRTM-DEM (which is actually a digital surface model; cf. Figure 4.3), the ASTER-DEM (which also is a digital surface model) and the very high resolution Japanese DEM (that we do not know how was generated or what kind of data it is based on).

As one can see, the SRTM-based inundation modelling consequently overestimates the inundation distance, while the ASTER-based inundation modelling clearly underestimates the inundation distance. The inundation modelling based on the very high resolution Japanese DEM data is generally still overestimating inundation distances, but not as consequently as the SRTM-based modelling.

The big difference of using the Japanese DEM-data lies in the level of detail that can be achieved in the modelling when using these data. An example of this can be seen in Figure 4.5. On the right panel, featuring the shaded terrain information with

superimposed inundation modelling results, one can see a road (linear white feature) which obviously is elevated as compared to the surrounding terrain, thus forming a natural barrier. However, where there are bridges the water should pass below these (example shown in left panel). Therefore, bridges were removed in the data in order to give correct effects during the inundation modelling.

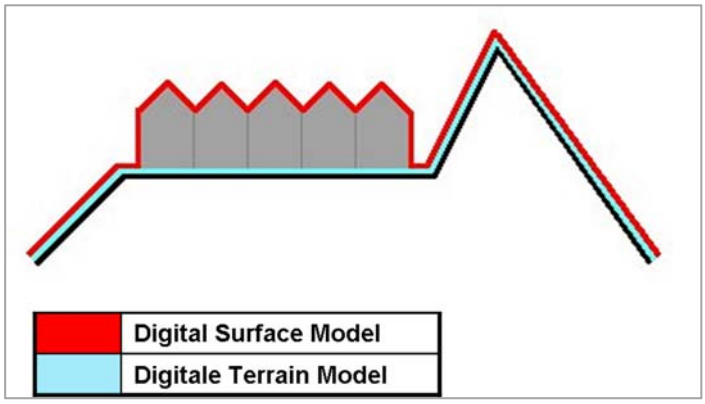

Figure 4.3: Surfaces represented by a Digital Surface Model and Digital Terrain Model. Source: http://en.wikipedia.org/wiki/Digital_elevation_model, image author: Martin Over, January 21, 2011.

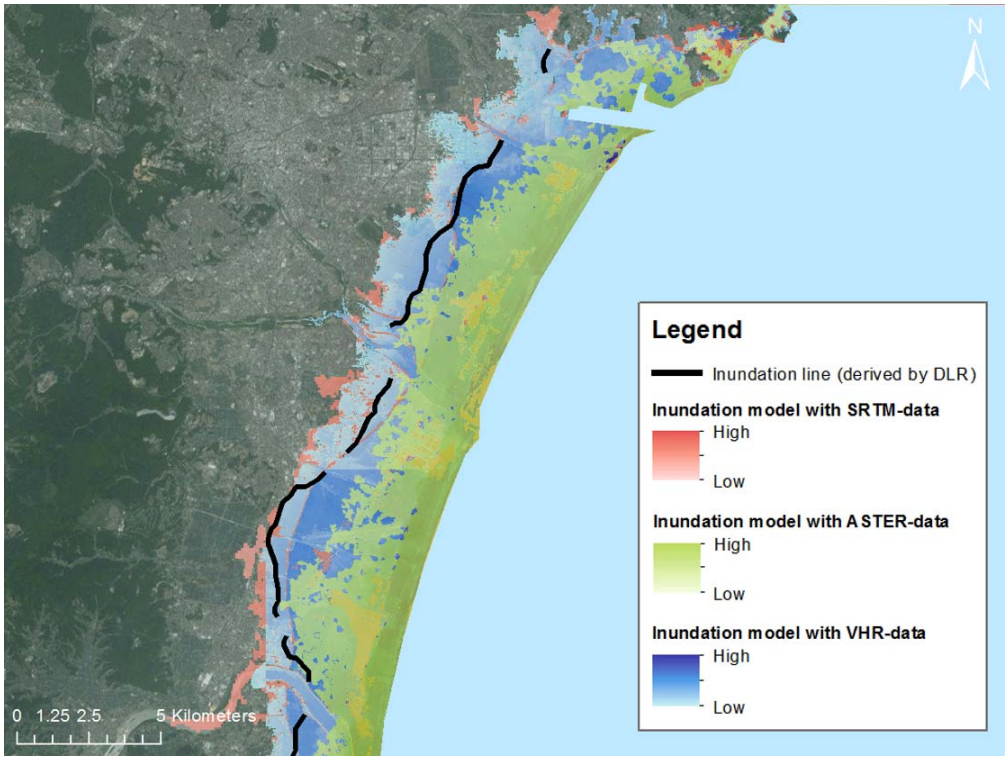

Figure 4.4: Influence of DEM resolution and quality on the inundation modelling. The three scenarios are FD_scenario D_v13_SRTM_DEM, FD_scenario D_v13_ASTER DEM, and the very high resolution (VHR) FD_scenario D_v13_ Post_dem, cf. Table 4.1.

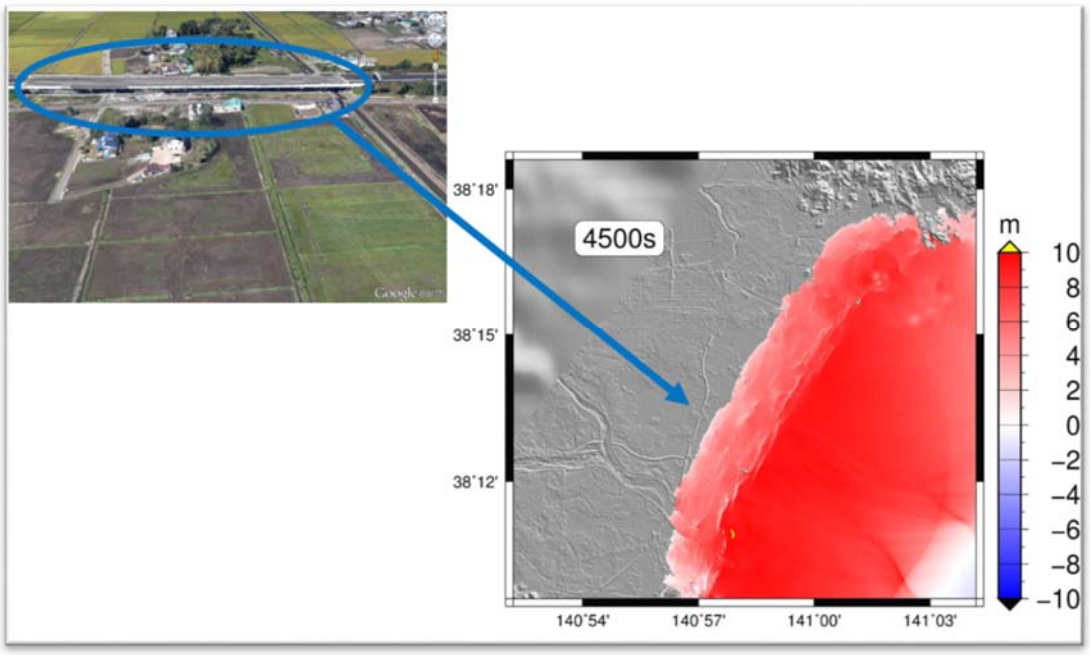

Figure 4.5: Comparing observed details in the very high-resolution Japanese DEM-data with StreetView in GoogleEarth.

5 Tsunami inundation modelling

The tsunami modelling is performed in two stages. First, the initial elevation due to the earthquake is given as input to the tsunami propagation model (GloBouss, see Pedersen and Løvholt, 2008). This model is capable to compute nonlinear and dispersive effects of tsunami propagation. The model computes the tsunami from the source area to the shoreline of Japan. The results from the propagation model is then conveyed into the tsunami inundation model ComMIT (Titov et al., 2011). With the latter model the inundation is calculated. For the tsunami propagation we have applied the GEBCO '08 dataset with a resolution of 0.5 arcmin (about 900 m), however extrapolated for use in the tsunami model to a resolution of 1 arcmin (about 1800 m). The resolution of the background data for the topography used in the tsunami inundation is about 2-6 m. For more details regarding the topographic data, see Section 4. In the inundation modelling, the datasets for the topography and the bathymetry (GEBCO '08) are combined and extrapolated to grids with a resolution of 22.2 m x 17.5 m on the finest grid level. The grid is first filled with data from the high-resolution topography. Grid cells without data are then filled with data from the GEBCO ’08 dataset. With inaccurate representation of the shoreline in the latter, this procedure will give possible smaller areas of dry land where it should be sea, see e.g. Figure 6.6. However, the effect of these artefacts is found to be limited.

The applied earthquake source is based on the knowledge of the 2011 Tōhoku earthquake. The seabed deformation is calculated by the formula of Okada (1985),

and the deformation is copied to the sea surface and used as an initial condition for the tsunami model. Adjustments to the source are made to improve the match with the observed surface elevation at the DART buoys (Løvholt et al. 2012). The earthquake source applied in this study is shown in Figure 5.1. The maximum surface elevation (both locally and for the entire Pacific Ocean) during the tsunami propagation stage is found in Figure 5.2 together with the location of the DART buoys. During the simulation the surface elevation is recorded in the numerical model at the same locations as the DART buoys (mariograms). The results from the modelling and the observations at the DART buoys are compared at eight different locations, see Figure 5.3. In the figure, the results for the tsunami propagation model are shown for both the linear hydrostatic (curve labelled "LSW") and the linear dispersive ("disp") modes. The numerical simulations mimic the registered tsunami quite well, and for the most distant DART buoys (e.g. 43413) the effect of frequency dispersion is apparent.

The inundation modelling is performed for seven different domains along the east coast of Japan, from 37. 8° to about 39.0° N, Figure 5.4. As an example of the inundation modelling results, we consider domain 7. Some snapshots of the surface elevation during the simulation of the inundation are found in Figure 5.5. The tsunami arrives Sendai about one hour after the earthquake. The maximum flowdepth and maximum inundation height of the tsunami at Sendai are shown in Figure 5.6. The maximum flowdepth is more than 10 m close to the shoreline. As shown, the road marked with red arrows reduces significantly the tsunami inundation. Here the flowdepth is reduced by about 3 m (from 6 m). The maximum surface elevation (in the sea) and the maximum inundation height (on land during) measured from still water are highest at the shoreline (about 10 m) and is reduced inward down to about 3-4 m at the trimline.

The convergence for both the tsunami propagation and the tsunami inundation model is thoroughly tested to confirm the reliability of the results.

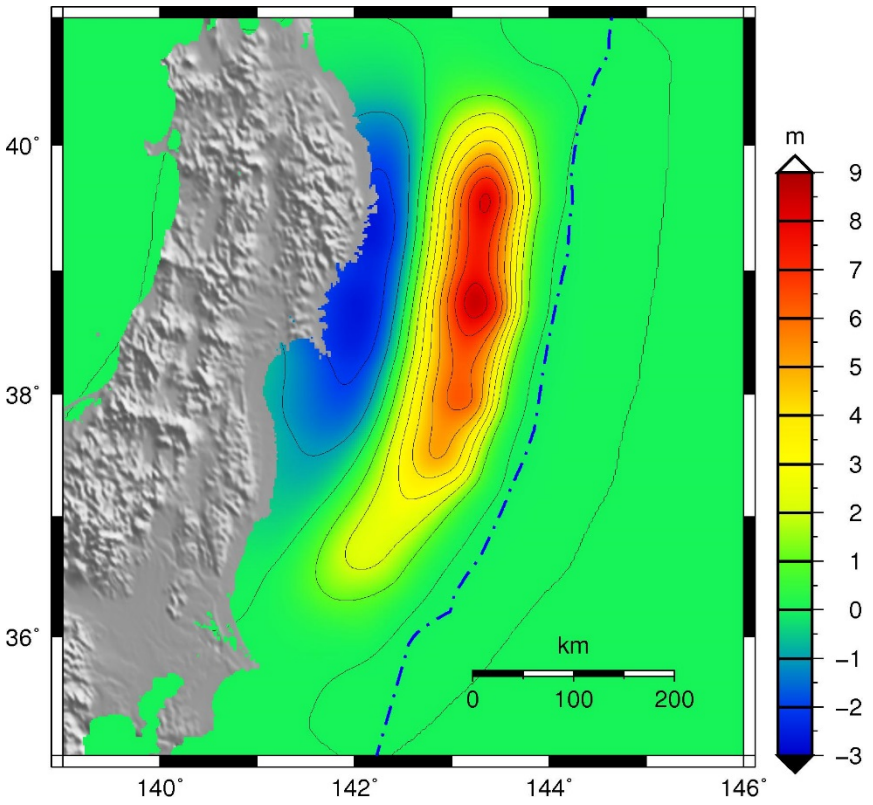

Figure 5.1: The initial sea surface elevation for the present study. Blue dashed-dotted line is the fault line for the 2011 Tōhoku earthquake.

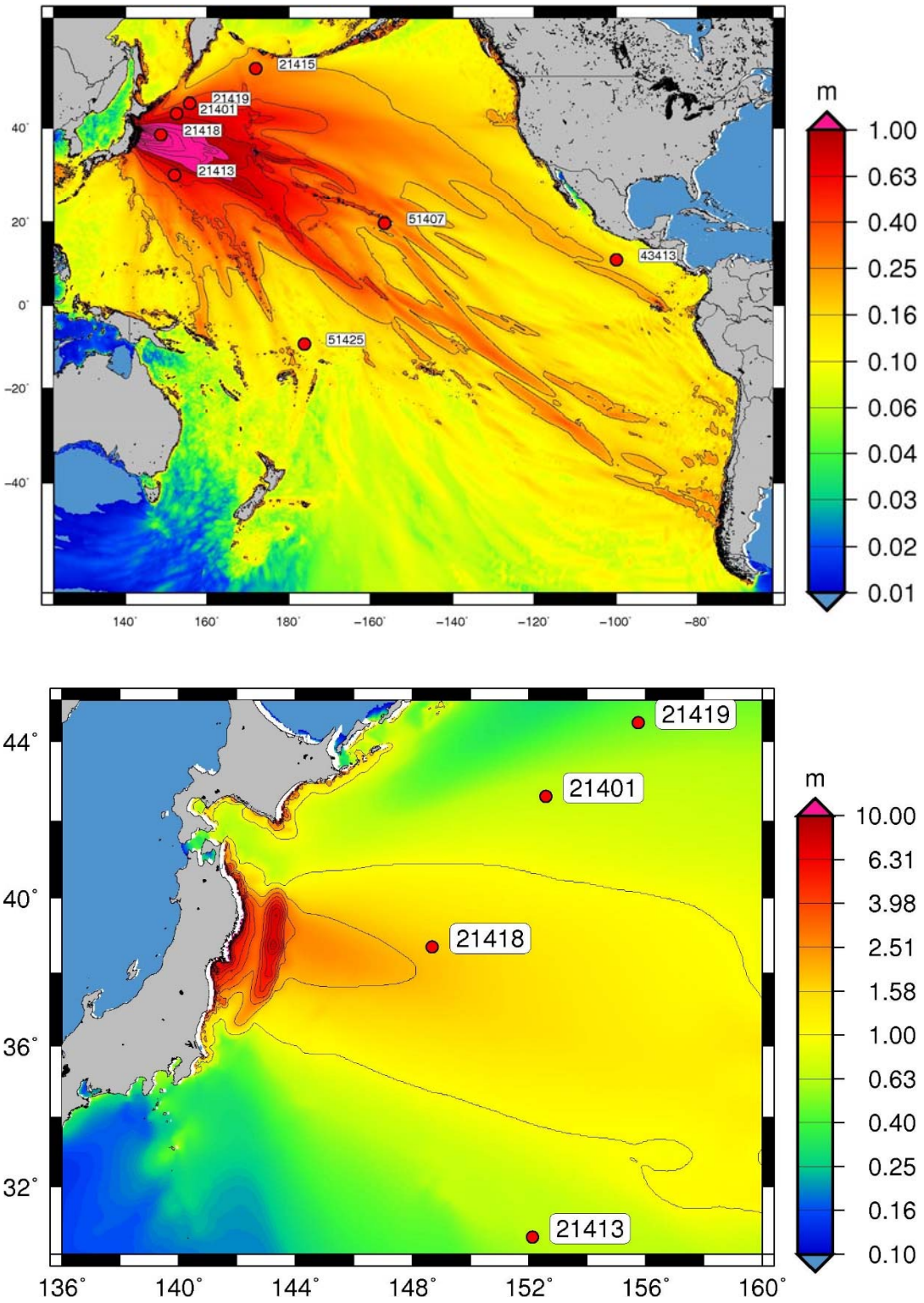

Figure 5.2: Maximum surface elevation during the computational time. Locations of DART buoys are given. The lower panel shows a zoom-in on Japan.

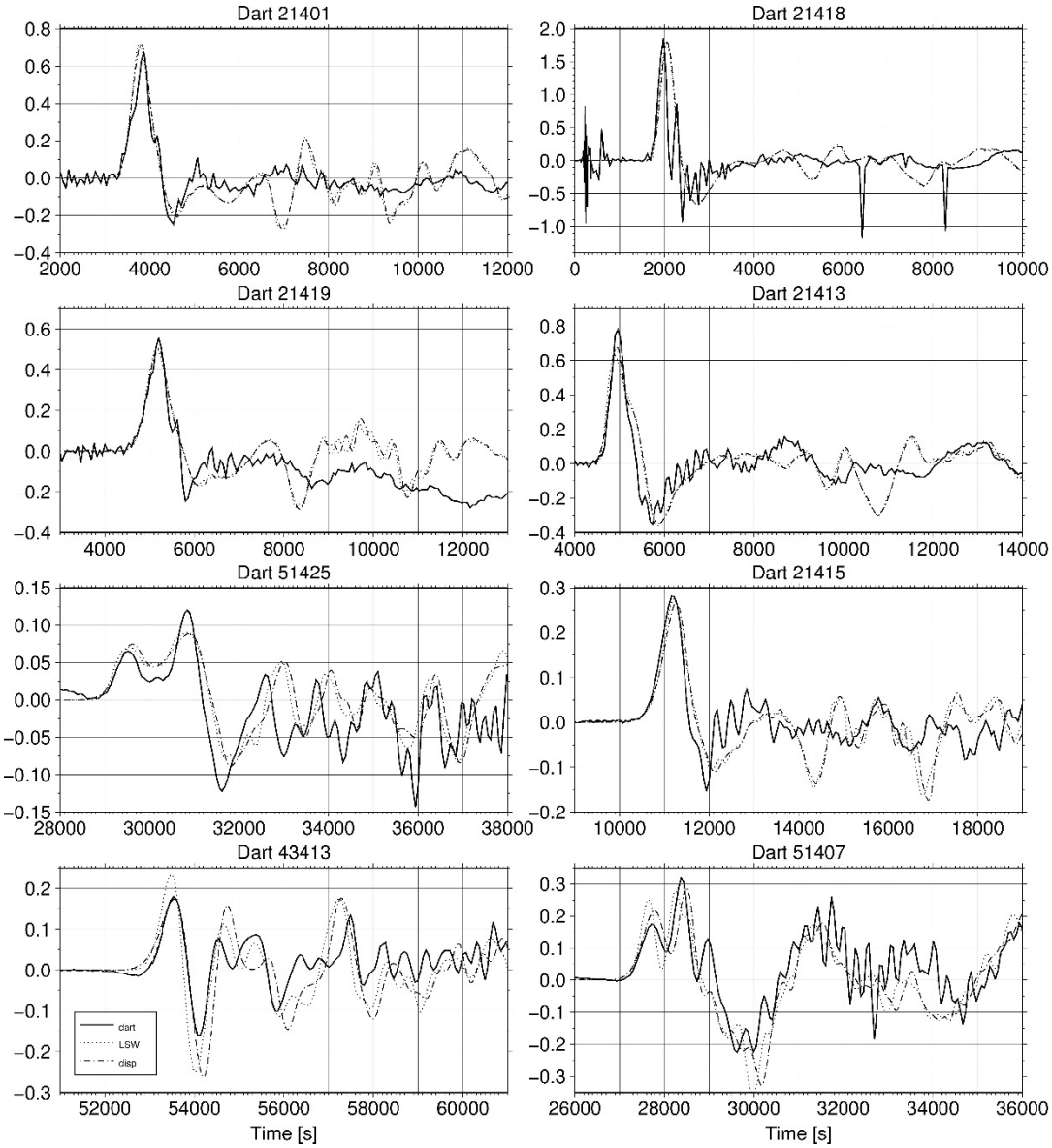

Figure 5.3: Mariograms at eight DART buoys, see Figure 5.2 for locations. The black line is the observed surface elevation at the respective DART buoy, the dashed line and the black line are the surface elevations for the linear hydrostatic (LSW) and linear dispersive (disp) version of the tsunami model, respectively.

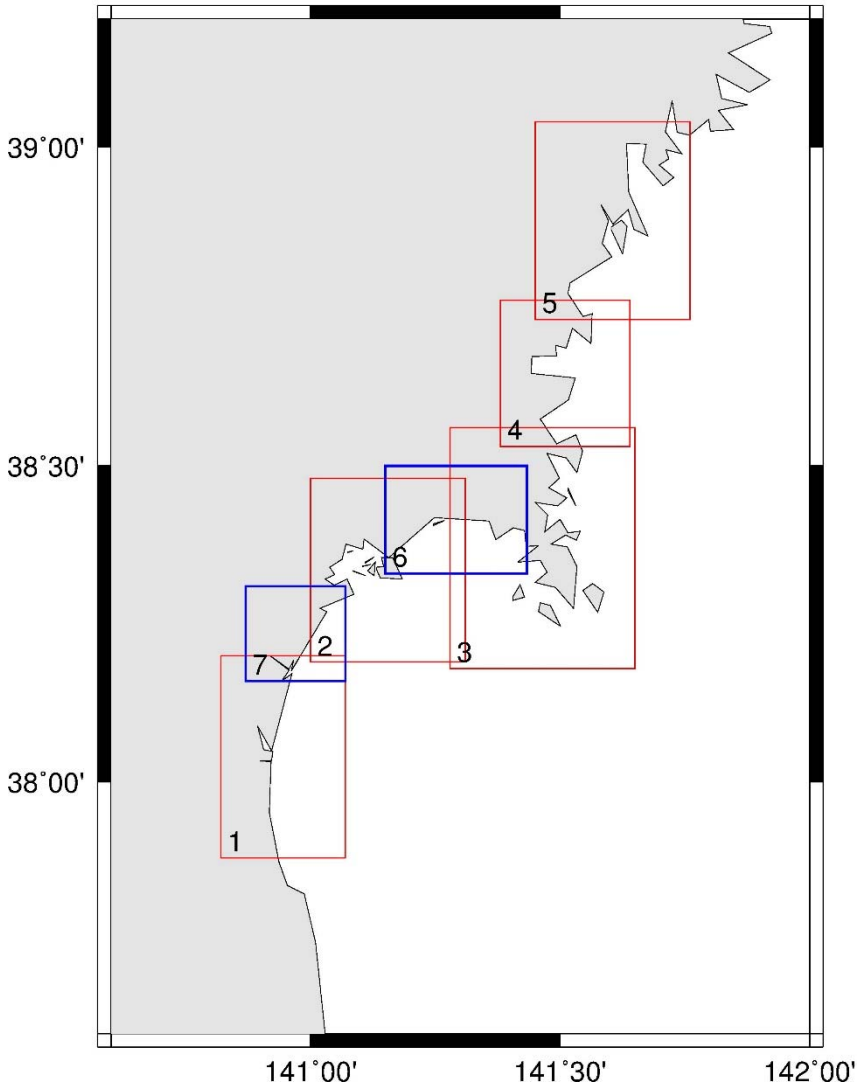

Figure 5.4: Overview over the different computational domains where the run-up is calculated. Ishinomaki is located in domain 6, Sendai is located in domain 7.

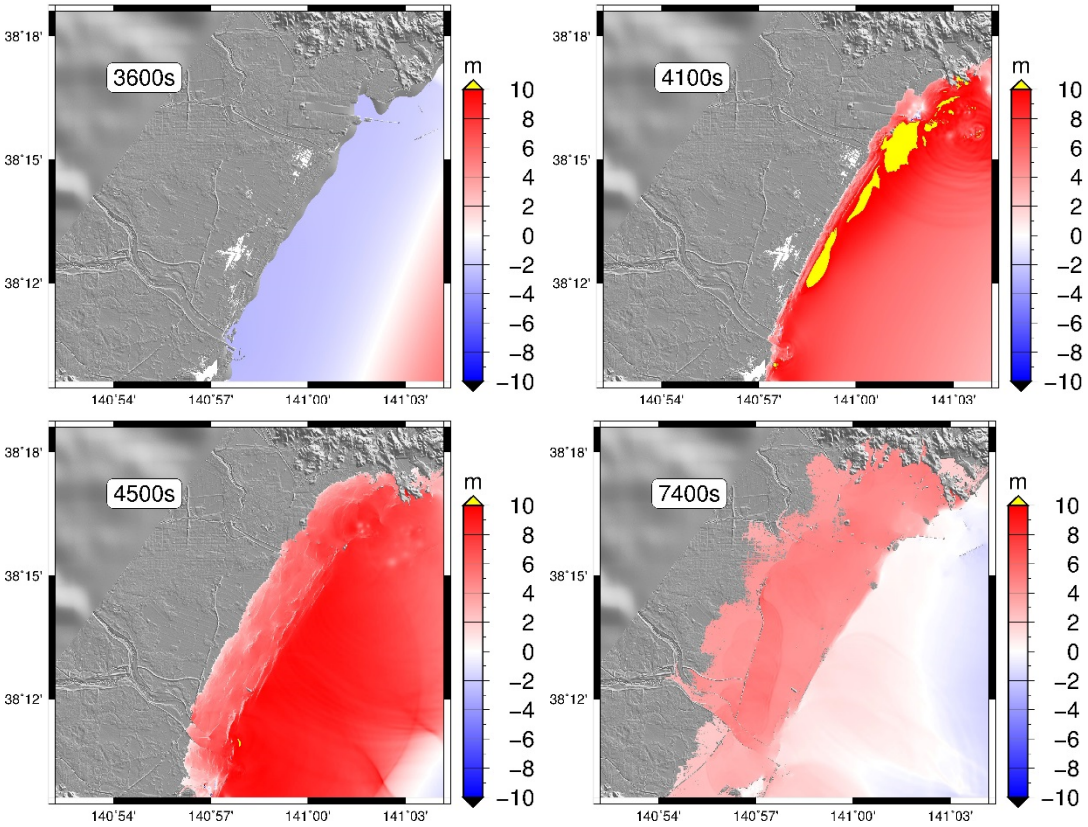

Figure 5.5: Snapshot of the tsunami inundation for section 7 at 3600 s, 4100 s, 4500 s, and 7400 s after the earthquake. Surface elevations above 10 m is coloured yellow.

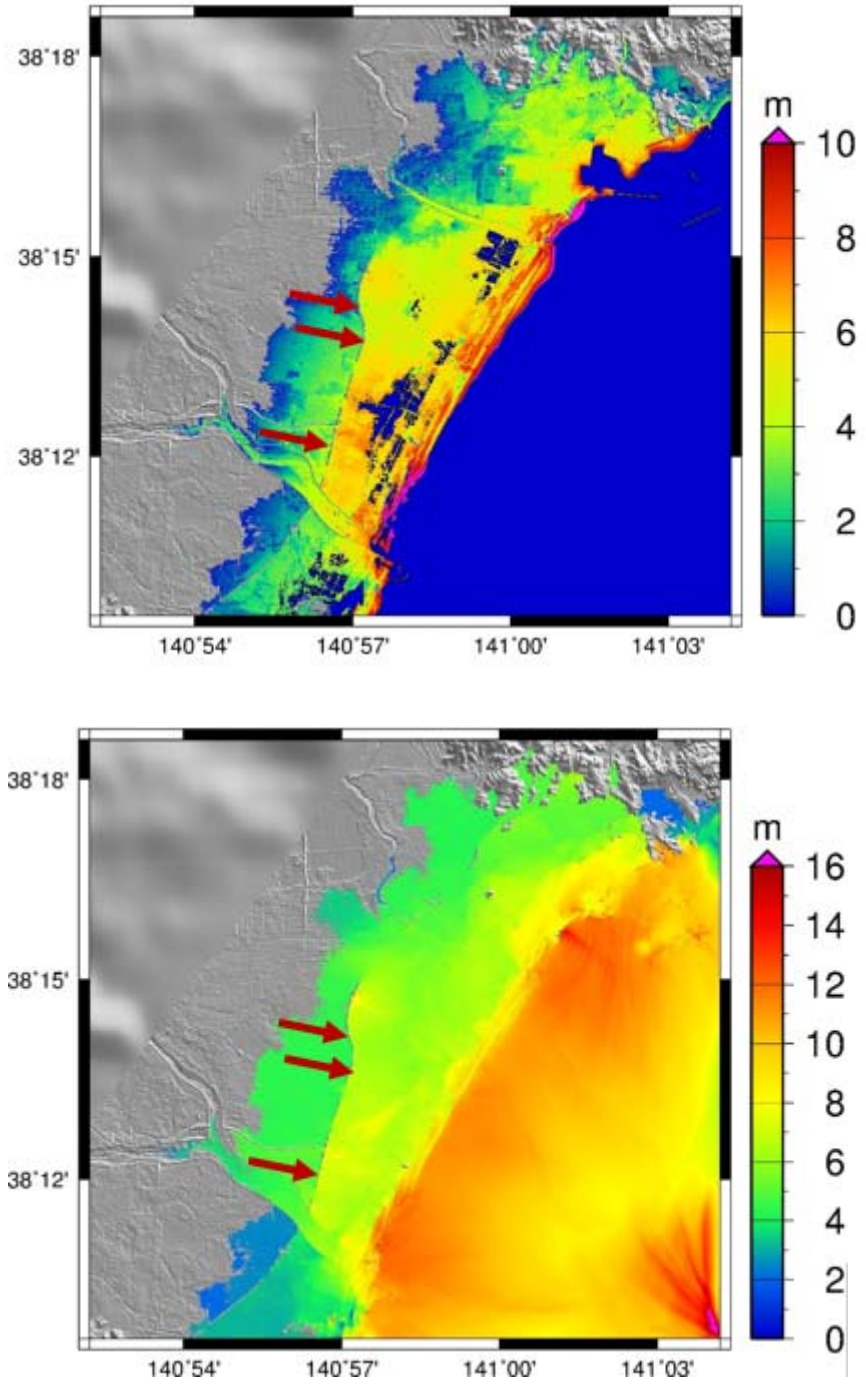

Figure 5.6: The maximum flowdepth (upper panel) and the maximum surface elevation in the sea as well as the maximum inundation height on land (lower panel). Red arrows shows the location of a road that reduces the tsunami run-up.

6 Mortality risk calculation

As mentioned in section 3.2 the final outcome of our GIS-based tsunami risk model is spatial information on mortality risk (loss estimates). Risk is expressed as *'hazard'* multiplied by *'consequence'* where *'consequence'* is defined as *'exposure'* multiplied by *'mortality'*.

Empirical data show a correlation between maximum flow depth and the percentage of people killed (Figure 6.3; Berryman et al., 2005; Suppasri et al., 2012; see also surveys by NGI, 2011; Løvholt et al., 2014; METU 2015). Dunbar et al. (2011) made a first analysis of the correlation between the number of fatalities and the measured run-up and inundation heights in Japan. Figure 6.1 shows, that there is a correlation between the number of deaths and the water level, which is rather obvious, considering that more than 90% of the fatalities were due to drowning.

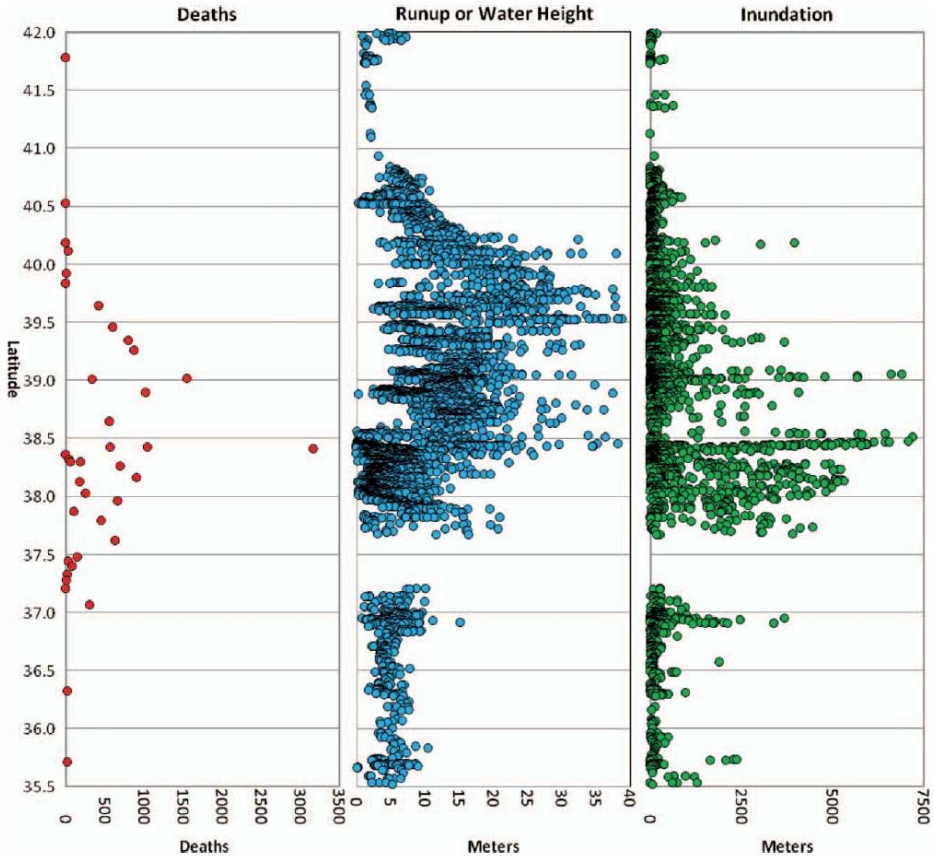

Figure 6.1: Latitude-based graphs of total deaths for selected principalities and prefectures, run-up or maximum water height, and maximum inundation distance from the 2011 Tōhoku tsunami (from NGI, 2011; Source: Dunbar et al., 2011, after IOC, 2011 – deaths; Mori et al., 2011 – run-up or water height and inundation distance).

Based on previous modelling (NGI, 2011; Løvholt et al., 2012), only rough estimates could be made on a correlation between flow depths and the number of fatalities in certain villages. In Figure 2.1 the modelled surface elevation as well as the measured run-up heights are plotted in bars. The yellow numbers provide the number of deaths and missing by community according to EERI (2011). Figure 2.1 further shows the highest absolute number of deaths and missing in Ishinomaki, which is a densely populated town close to the shore. Although water levels were lower here than in many other areas, the high population density and most likely also debris from collapsed buildings, that has shown to considerably contribute to loss of life and damage (Dalrymple et al., 2006), are supposed to have contributed to the high number of fatalities. Videos from the Tōhoku tsunami available online showed that a huge amount of wooden houses collapsed in the area. After collapsing they were transported inland with the water causing further damages by crushing into other buildings and crumpling people. Even though Ishinomaki has the highest absolute number of fatalities, the percentage is quite small due to the size of city. The fact that a comparably small area was flooded might underpin that the effect of flotsam is rather significant.

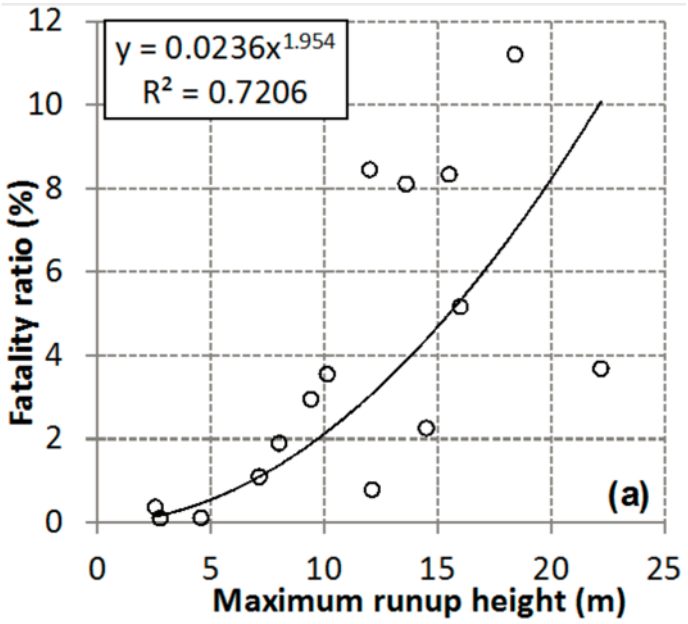

Figure 6.2: Relationship between maximum run-up height and fatality ratio based on data from Miyagi prefecture (from Suppasri et al., 2012).

Suppasri et al. (2012) developed some basic fatality ratio curves based on statistics and their field data (Figure 6.2). The flow depth can, therefore, be used for the calculation of a mortality percentage map, i.e. the percentage of the people present (in each raster cell) expected to perish due to a given flow depth.

The input data thus needed are:

- flow depth (as a representation of the hazard)

- vulnerability (in order to pick "correct" S-curve and calculate mortality risk, see below)
- exposure (in order to calculate mortality)

Calculation of total mortality is based on empirical data accessible through literature research. The data are used to derive a relation between flow depth and mortality with upper and lower bounds to include the uncertainty in the data and the influence of other parameters, such as, e.g. physical environment and vulnerability, on the mortality (Eidsvig et al., 2009, cf. Figure 6.3Figure 6.3). Flow depth is the most important, but not the only parameter influencing the mortality (current velocity, flotsam, etc., also play an important role). The possible mortality values for one flow depth are between the lower and upper bound of the mortality (flow depth relation).

In our approach, the vulnerability (here structural building vulnerability as described by NGI, 2009a) is used to pick the "correct" S-curve (cf. Figure 6.3), e.g. if the S-curve at a given flow depth returns a mortality $M \in [0.2, 0.8]$ and the building vulnerability is = 0.25, the total mortality is calculated as:

$M = mort_{lower\text{-}bound} + vuln \times (mort_{upper\text{-}bound} - mort_{lower\text{-}bound})$

i.e.: $M = 0.2 + 0.25 \times (0.8\text{-}0.2) = 0.35$, cf. Figure 6.3Figure 6.3.

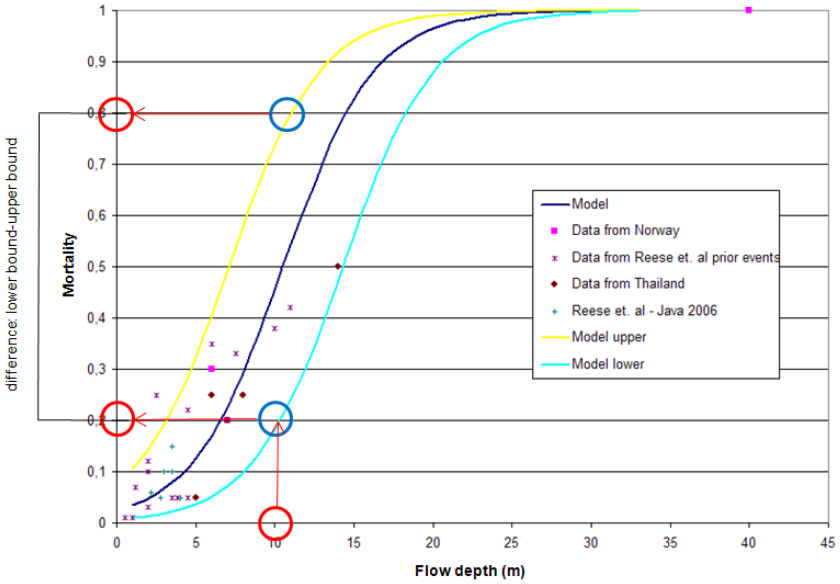

Figure 6.3: Relation between flow depth and mortality (from Eidsvig et al., 2009; data collected from EEFIT, 2006; Jørstad, 1968; Reese et al., 2007).

The resulting percentage map, i.e. the mortality risk-map is then used to calculate the number of fatalities, by combining the percentage map information with the average population density map.

6.1 Hazard (Flow depth raster)

The hazard used in this study is represented by the maximum flow depth as hindcasted for the 2011 Tōhoku tsunami (for details on the inundation modelling, see Section 5). The flow_depth dataset is a raster dataset with a spatial resolution of 23 m x 23 m (resampled from the 22.2 m x 17.5 m flow depth grid in order to be usable within a GIS environment), where the value of each cell represents the maximum flow depth at a given location. The flow depth modelling result for the Miyagi Prefecture is visualized in Figure 6.4.

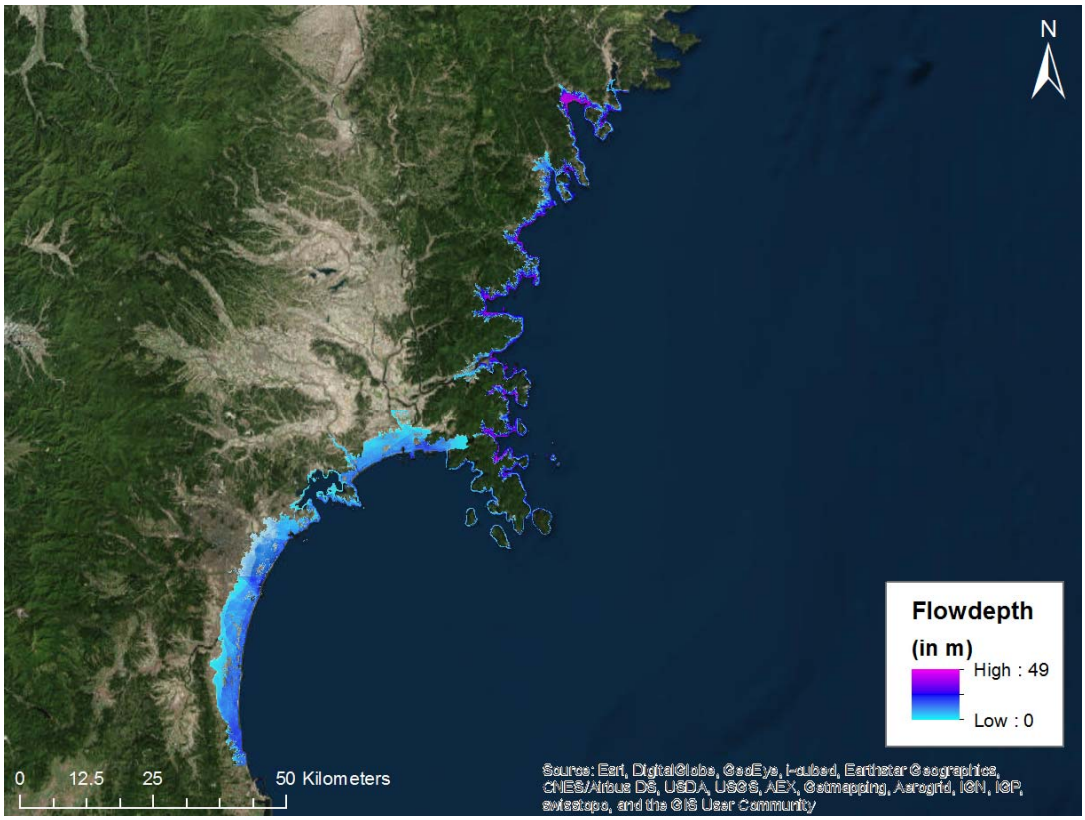

Figure 6.4. Maximum flow depth, Miyagi Prefecture.

Note that buildings and infrastructure are not included in the simulation, since these data were not available to us in a feasible format in time. Especially for densely urbanized areas, access to such data would have been very favourable. In laboratory experiments, e.g. Bridges (2011) could show that variations in the grouping of macro-roughness elements affect the inundation response. In particular, increasing the alongshore spacing between a pair of macro-roughness elements caused the force and run-up to exceed the baseline values in several groupings. These results suggest that the relative spacing of neighbouring buildings could have substantial influence on the tsunami inundation forces further inland (cf. Figure 6.5). Kaiser et al. (2011) showed similar effects for different land-cover roughness scenarios at Patong Beach, Thailand.

There were different datasets available to compare and validate our inundation modelling results. These were namely data from the "Reconstruction assistance research archive", available at http://fukkou.csis.u-tokyo.ac.jp/, specifically the datasets Water marks and Inundation area, and building damage data available from WorldMap/Center for Geographic Analysis at Harvard University (http://worldmap.harvard.edu/japanmap/) (cf. Table 4.1).

In the following, we show a qualitative comparison of the modelled flow depth and the above mentioned datasets exemplified for the city of Ishinomaki, Miyagi Prefecture.

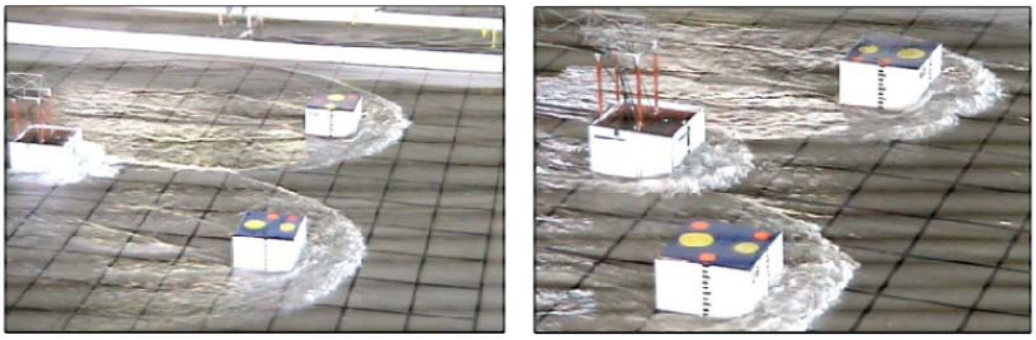

Figure 6.5: Influence of macro-roughness on tsunami run-up and forces. Image source: Bridges (2011).

6.1.1 Comparison with datasets «Inundation area» and «Water marks»

Figure 6.6 shows a comparison between the modelled flow depth and the dataset inundation area. Figure 6.8 shows again the flow depth, this time with the superimposed values of the dataset water marks. Two photographs illustrating how the height information given in the dataset water marks was measured are shown in Figure 6.7.

In general, the agreement between our modelling results and the field data available from the "Reconstruction assistance research archive" is good. Our flow depth values are generally a bit higher than the measured water marks. Deviations are in the order of 0.5 to 1.5 m, depending on the area and the simulation run. Due to slightly different «flattening» filters used, the results of the simulations differ slightly from each other. As mentioned earlier, it is important to note that buildings and infrastructure were not included in our flow depth simulations.

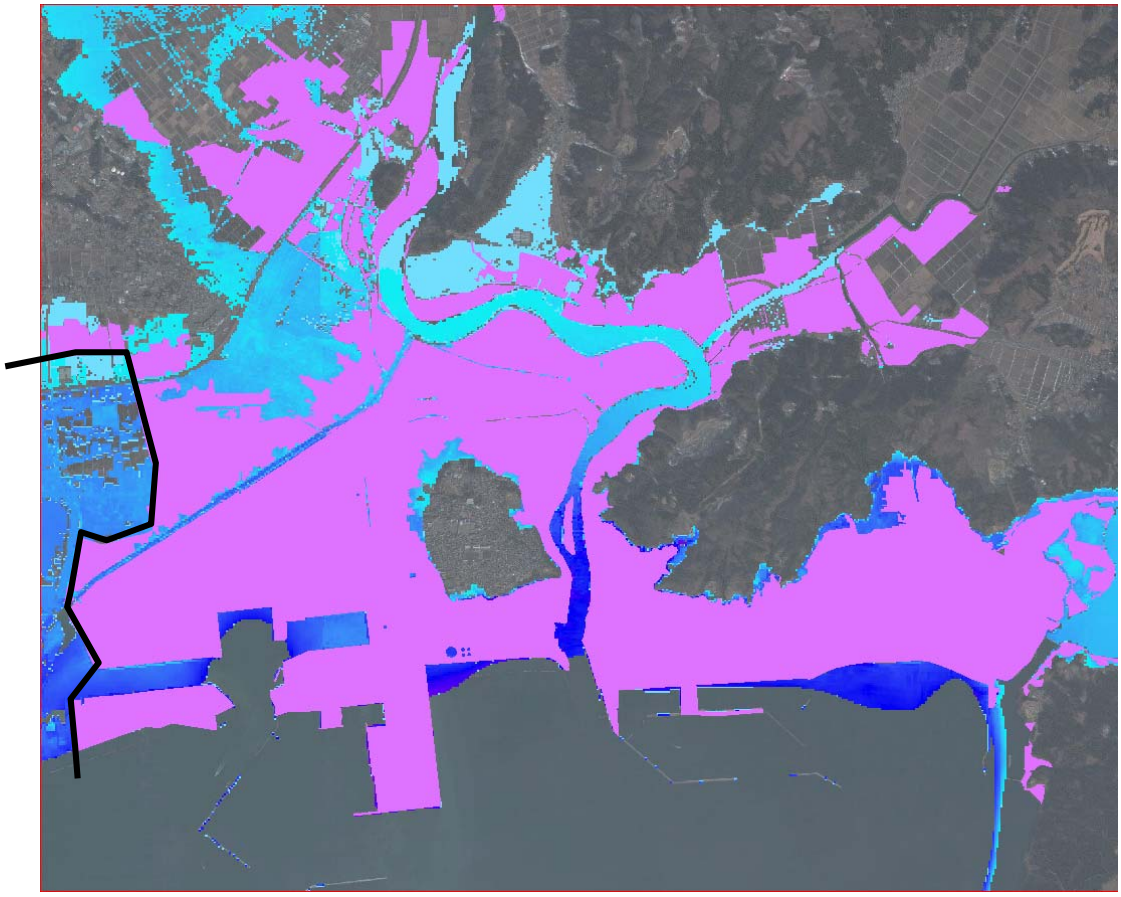

Figure 6.6. Flow depth *superimposed with post-tsunami field data* inundation area *(in purple). Zoom-in over southern part of Ishinomaki city. Black line = Ishinomaki city border. The different shoreline in the modelling and in the post-tsunami field data (purple) is due to coarse and inaccurate values on land in the GEBCO data (the shoreline is inaccurate).*

Figure 6.7. Measurement of height information as given in the dataset water marks*. Photography available on http://fukkou.csis.u-tokyo.ac.jp/, Copyright © 2012, Reconstruction assistance research archive secretariat.*

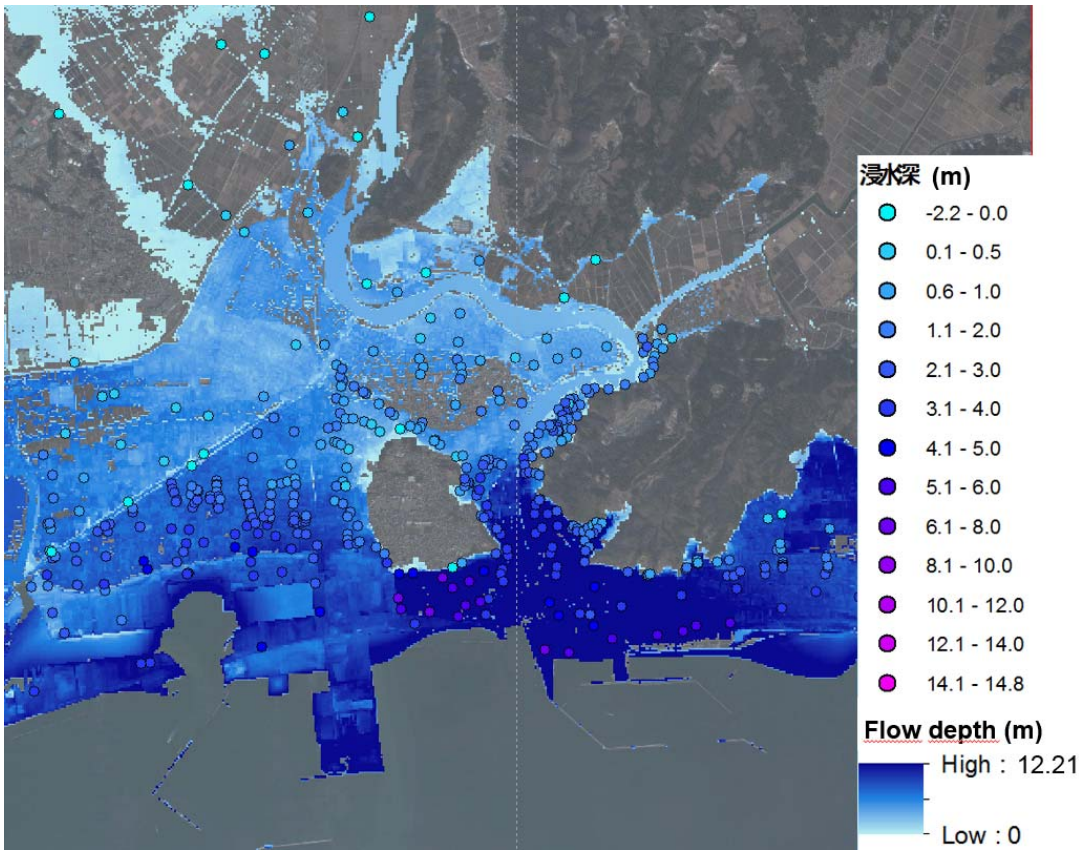

Figure 6.8. Comparison between Flow depth *and post-tsunami field data* water mark *(superimposed point symbols, see legend for values in metres). Zoom-in over southern part of Ishinomaki city.*

6.1.2 Comparison with dataset «Building damage»

Figure 6.9 shows a qualitative comparison between the modelled flow depth and the building damage data available from WorldMap (Harvard University). This qualitative comparison clearly shows that the areas with the highest modelled flow depth correspond well with the areas where the highest building damage was recorded.

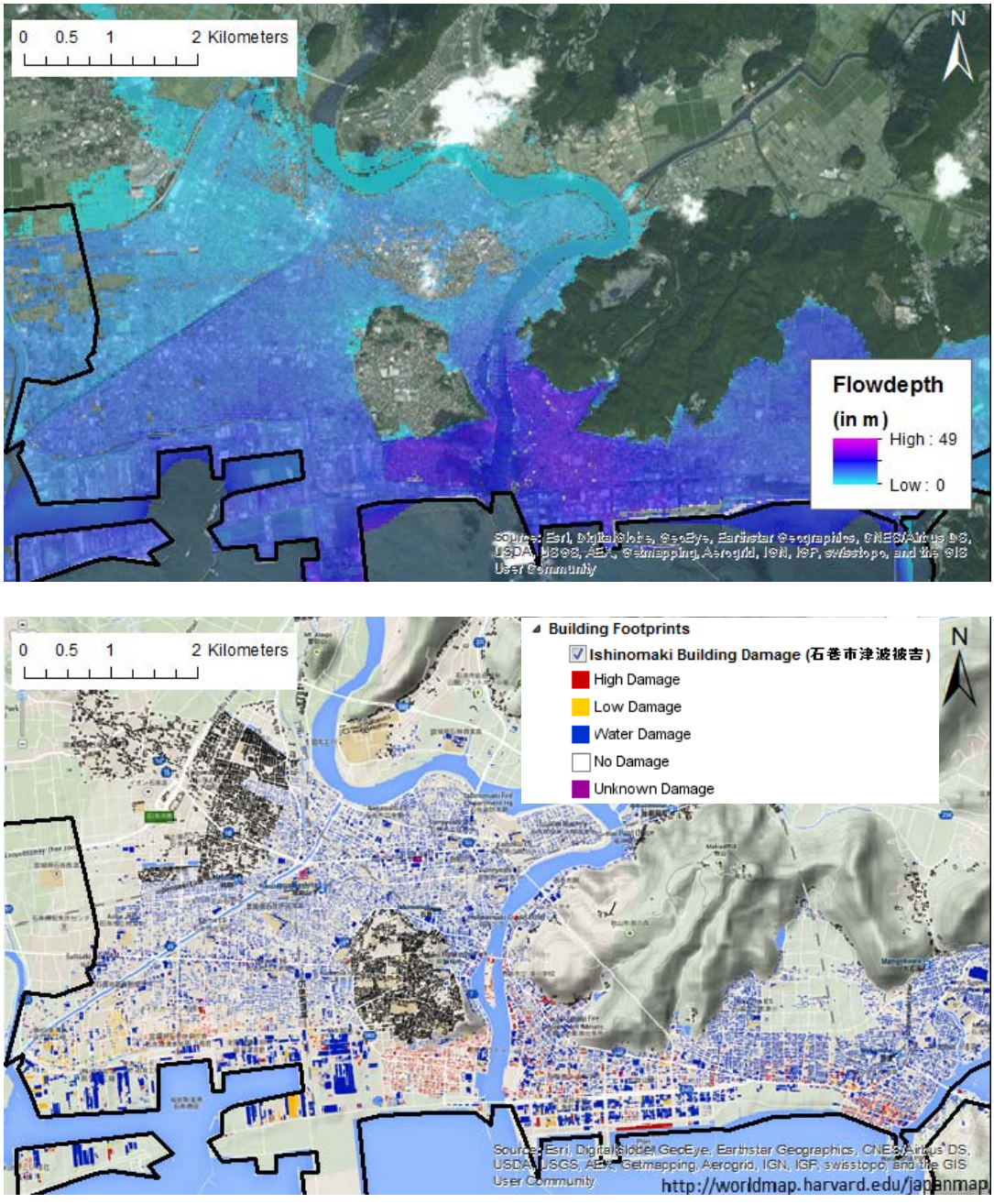

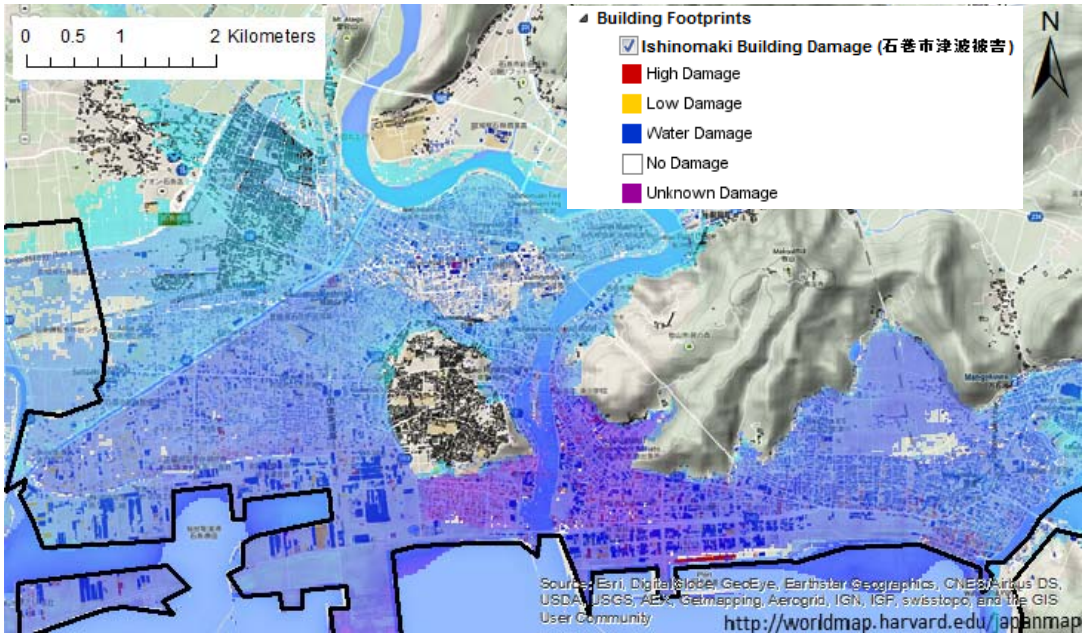

Figure 6.9: Modelled flow depth compared to building damage data from WorldMap, Center for Geographic Analysis at Harvard University (http://worldmap.harvard.edu/japanmap/). For better visibility we show both flow depth (upper panel); building damage data (middle panel) and the superimposed combination of both datasets (lower panel). Black line = Ishinomaki city border.

6.2 Vulnerability

Vulnerability can be expressed as the possibility of an element at risk (a person, a village, an economic value) to be damaged or destroyed by a hazard. There exist many different concepts to choose vulnerability indices (see surveys by González-Riancho, 2014b; METU, 2015). Some authors concentrate on physiogeographic features (e.g. Doocy et al., 2007; Sinaga et al., 2011), while others concentrate on vulnerability as a function of land-use (e.g. Najihah et al., 2014). In our model we focus on the structural vulnerability of the built-up environment, an approach presented by, e.g. Dominey-Howes and Papathoma (2007).

Our GIS model is designed in a way that vulnerability can be fed into the model on a cell-by-cell basis, alike the other input parameters. In principle, our approach requires that information on building vulnerability is available (e.g. NGI, 2009c). By the time we had to finalize our modelling within the RAPSODI project, building vulnerability was unfortunately not available to us in an appropriate format. In order to nevertheless run the model for the 2011 Tōhoku event, we introduced a synthetic vulnerability layer based on the built-up area within the Ishinomaki city boundaries (Figure 6.10). In this layer, all cells covering areas with buildings were assigned a vulnerability value. Since we lacked information to differ between low (0) and high (1) building vulnerability, a uniform building vulnerability value was assigned to all

of these cells. We performed two different model runs, one where the uniform building vulnerability was set to 0.25, one where it was set to 0.5. Results are given in Section 6.4.

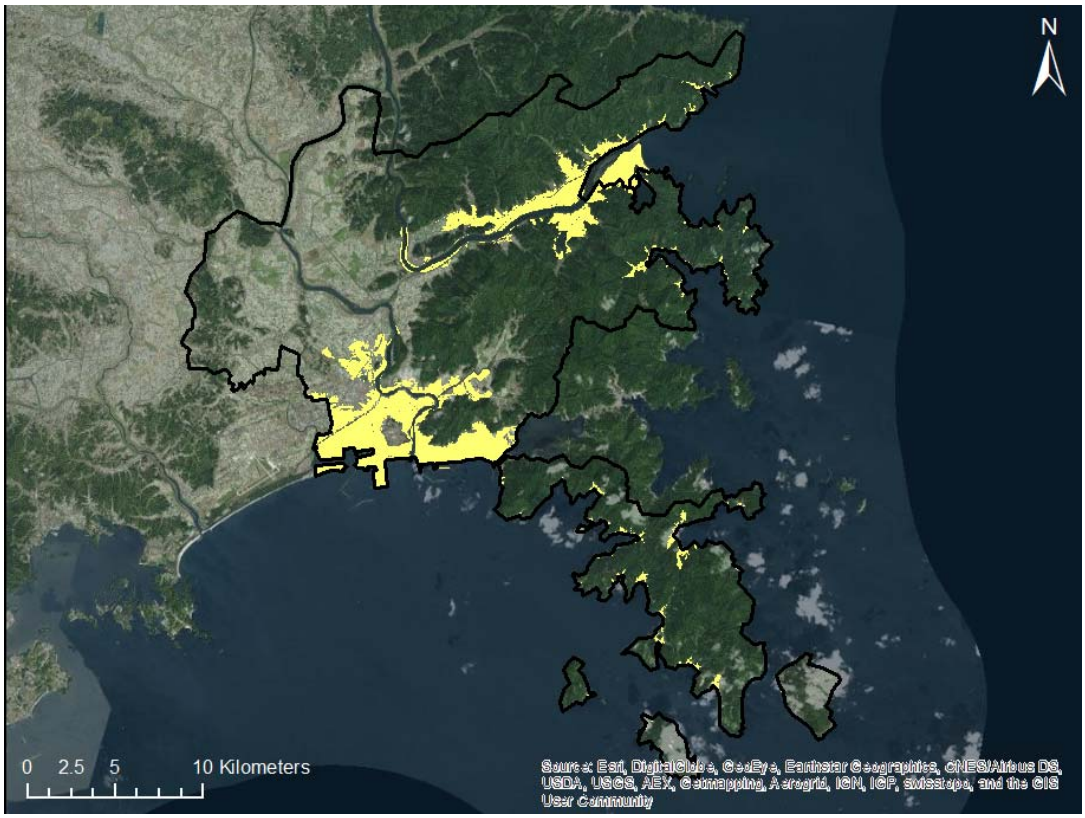

Figure 6.10: Synthetic vulnerability map for Ishinomaki city. A uniform building vulnerability was assigned to all built-up areas. Black line = Ishinomaki city border.

6.3 Exposure (Population raster)

People exposure and subsequent risk for the loss of lifes are difficult to predict due to the mobility of people during the day and during different times of the year, and due to peoples different behaviour during a disaster. Many circumstances have shown to influence the risk to life of individuals: flow depth and velocities, distribution of people, age of people, preparedness, risk perception, and many more (e.g. Penning-Rowsell 2005; González-Riancho et al., 2014b).

An analysis of the Tōhoku tsunami showed that in total 77.6% of the people who died in the tsunami were older than 50 years, and 46.5% were older than 70 years (Vervaeck and Daniell, 2011). Only 15% were younger than 30 years (Ogasawara et al., 2012). A distribution of age among the fatalities is given in Figure 6.11. This confirms the general statement that old people are more vulnerable since they often cannot evacuate themselves as fast as younger ones (and often do not want to). Seasonal changes can have influence on people exposure as the 2004 tsunami in

Thailand showed. Therefore, for more accurate risk and vulnerability assessment, people exposure and the other circumstances listed above have to be taken into account for different scenarios.

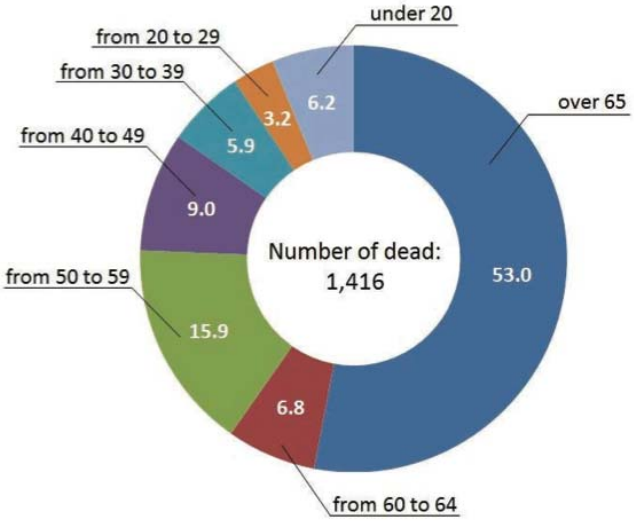

Figure 6.11: Age distribution among fatalities of the 2011 Tōhoku tsunami (Ogasawara et al., 2012).

In order to evaluate the human population exposure to the tsunami in our study, the population census data for 2010 were used. This population census data were kindly provided to us by Prof. Y. Maruyama, Department of Urban Environment Systems, Graduate School of Engineering, Chiba University, Japan. Population exposure is represented by the number of persons per 500 m x 500 m grid cells, which is the resolution of the aggregated census data. The data are explained in more detail by Maruyama and Tanaka (2014).

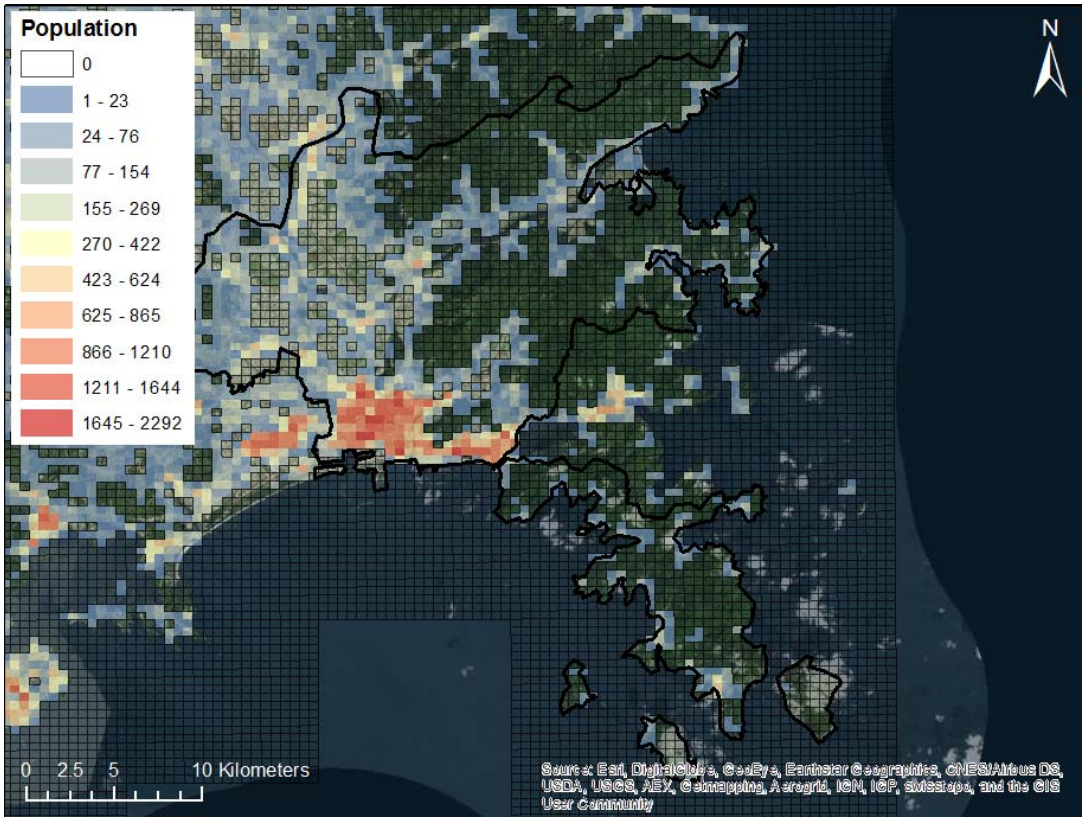

Figure 6.12: 2010 population census data for Ishinomaki. Data kindly provided by Prof. Y. Maruyama, Department of Urban Environment Systems, Graduate School of Engineering, Chiba University, Japan. Black line = Ishinomaki city border.

6.4 Case study: Ishinomaki

The mortality risk map and, subsequently, the calculation of the expected number of fatalities were carried out using the approach explained in the beginning of Section 6. Using the rasters flow depth and vulnerability explained above as input to the described model yields the mortality risk map shown in Figure 6.13. Combining the mortality risk map with the population raster (2010 census data) results in the mortality map, showing the modelled expected number of fatalities per grid cell (Figure 6.14).

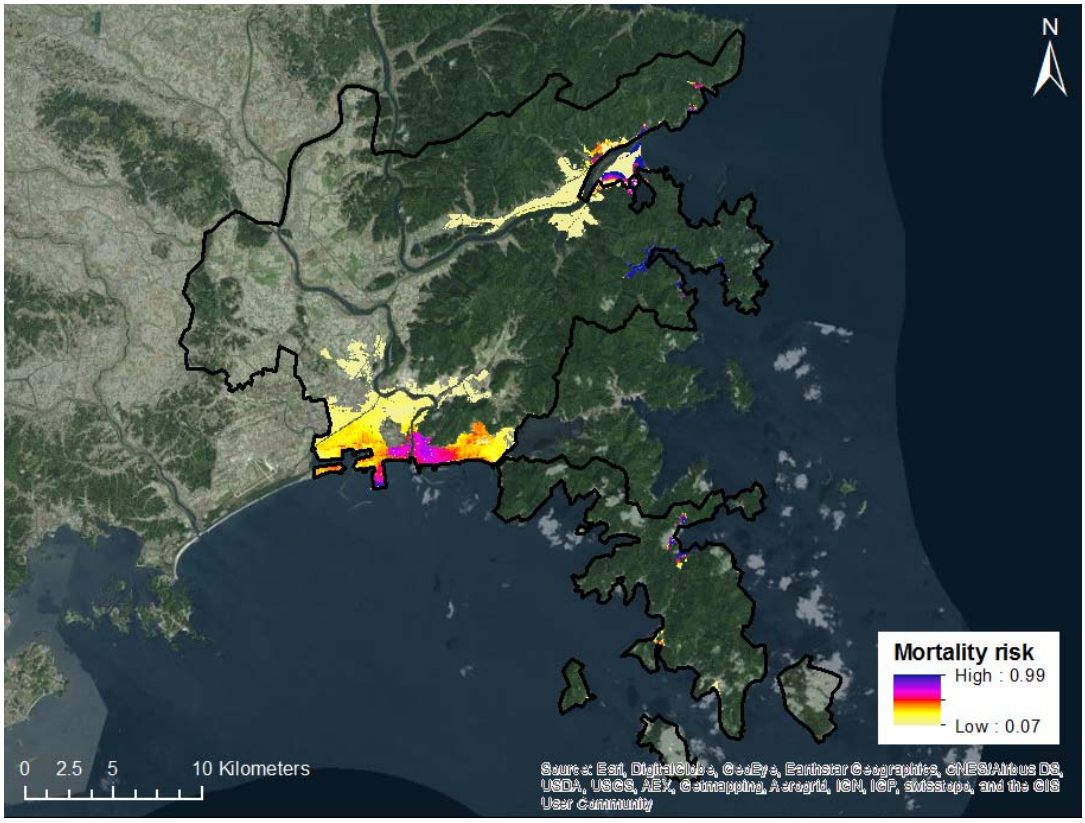

Figure 6.13: Mortality risk map. Black line = Ishinomaki city border.

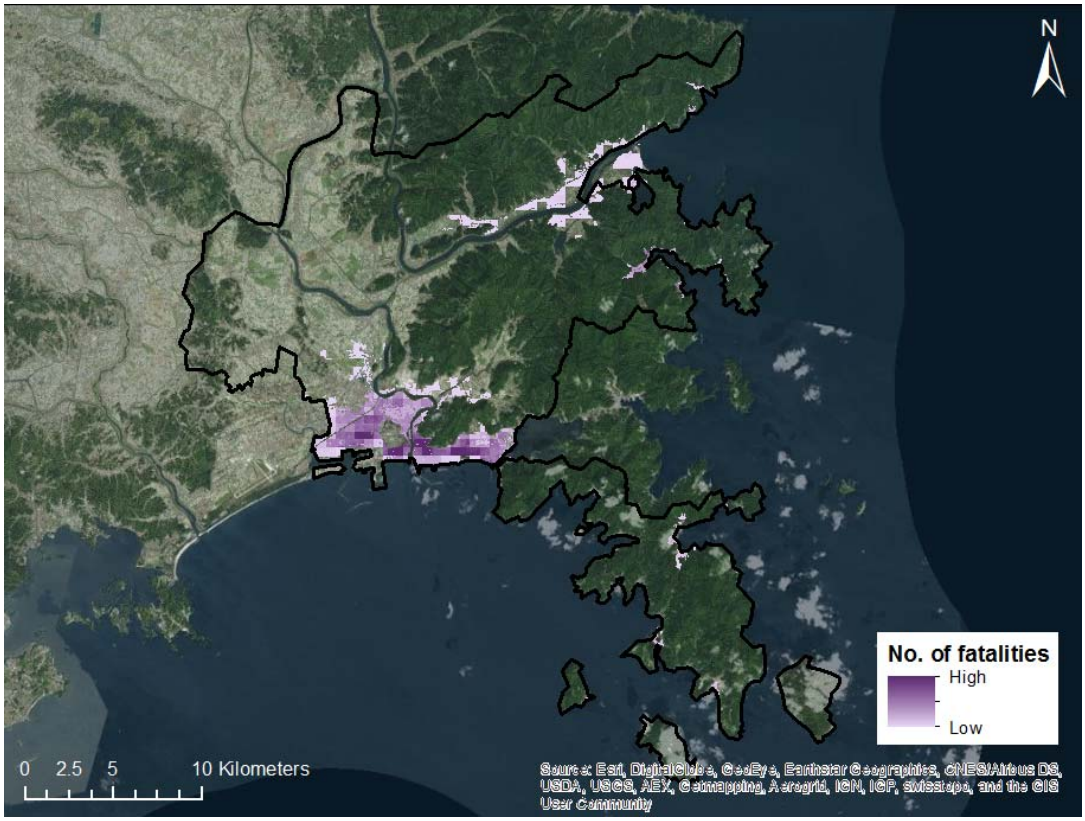

Figure 6.14: Mortality map. Black line = Ishinomaki city border. The coarse grid-pattern is a result of the fact that the population grid has a much coarser original resolution (500 m x 500 m) than the other datasets applied for the GIS analysis (23 m x 23 m).

Using a synthetic uniform building vulnerability of 0.25, the calculated expected death toll amounts to 2900 fatalities. Using a synthetic uniform building vulnerability of 0.50, the total expected number of fatalities is 5800. Reported actual death tolls for Ishinomaki city vary between 3000 (source: The Asaih Shimbun, March 11, 2013) to nearly 4000 fatalities (source: Ishinomaki Fund). What is clear is that Ishinomaki, located just 80 miles west of the epicenter, had the highest number of fatalities of all cities in the disaster. Of the total estimated death toll of 20 000 in Japan, approximately 20-30% (percentage depending on the considered information source) died in Ishinomaki.

A flaw of our approach is that in the census data population is only present in settlement areas (i.e. not in industrial areas by the harbour). This implies that our approach neglects all fatalities outside these settlement areas. This is obviously not true due to the severe damage and the high number of fatalities reported in nearshore working areas. Commuter data do exist and can be included in our approach, but such data were available too late to be implemented in the present study.

7 Conclusions

The maximum flow depth was obtained by hindcasting the 2011 Tōhoku earthquake and tsunami using knowledge of the earthquake source (Løvholt et al., 2012) and combining bathymetry data (GEBCO '08) with very high resolution Japanese digital elevation data. This flow depth was then used in a GIS-based tsunami mortality risk model in order to calculate tsunami mortality risk. The city of Ishinomaki was chosen for the validation of the model results.

The calculated inundation areas and flow depths both agree well with post-event field data. The modelled mortality in Ishinomaki city agrees reasonably well with reported death tolls, even though we had to introduce several simplifications into our model, such as uniform building vulnerability due to lack of available relevant data (the data were available too late, were not in appropriate formats, or did not cover relevant areas). It should also be noted that reported death tolls vary considerably (3000-4000, some sources, though of non-verifiable nature, report even higher numbers).

Our study showed that the GIS-based tsunami mortality risk model reasonably hindcasts mortality for the 2011 Tōhoku earthquake and tsunami, even with all the assumptions that had to be made. With the help of the model it is possible to identify high mortality risk areas, as well as identify the main risk driver(s) in high-risk areas, which often can be attributed to either high to very high flow depths, high population concentrations (causing high exposure), vulnerable building mass, or a combination of these factors. Also an earlier hindcasting calculation, this time for the 2009 American Samoa tsunami (Harbitz et al., 2011) showed satisfactory model performance.

Based on these positive hindcasting results we are confident that our model could form a useful tool within a tsunami risk reduction framework. The model can be run for different tsunami scenarios potentially impacting a given tsunami threatened area or town. The results of the model can be used, e.g. to produce maps showing different mortality risk scenarios that would have to be expected for different flow depth scenarios with corresponding probabilities. This could help in meaningful urban planning, allowing for the identification and selection of evacuation routes, evacuation locations, planning of mitigation structures, etc.

Accessing the large amount of potentially available post-disaster field data was more challenging than expected when carrying out the tsunami mortality risk modelling in the RAPSODI project. Several of the databases where relevant data are stored are in Japanese only, something which obviously hampers the access of the data for non-Japanese speakers. Other relevant data are stored without geographical information (e.g. in tables or as maps in PDF- or JPG-format). It would have required disproportional resources to convey this information into a utilisable format for use in the RAPSODI project.

Deliverable 7 “Results of the laboratory analysis and wave flume tests” (TU-BS, 2015) describes the RAPSODI laboratory experiments with various tsunami breakwaters under tsunami impact. The most well-functioning design is recommended for a possible implementation into the numerical model in order to study its influence on inundation and mortality risk. However, as overflow without breakwater failure is not realistic and because there is considerable flow through the structure (in addition to the overflow; Cappietti et al., 2012) it was decided not to implement synthetic breakwaters in a numerical model that presently cannot handle breakwater failure or permeability.

8 Possible extensions

The design of the GIS-based tsunami mortality risk model allows for the expansion of the model with new or other parameters, as well as for the refinement of already implemented parameters.

The flow depth modelling can be refined by including obstructions such as buildings and infrastructure. Such obstructions may locally increase the flow depths or canalise the water, hence locally intensifying the water current velocities and the wave loads. On the other hand, they may also increase the flow resistance and thus reduce the inundation distance. The specific momentum flux per unit width (expressed by the product of flow depth and water current velocity squared) is often considered the best damage indicator (Tsunami Pilot StudyWorking Group, 2006; see also discussions by METU, 2015). Comparing the computed specific momentum flux per unit width and damage data (e.g. data mentioned in Table 4.1) may enable further validation and improvement of the numerical model.

In addition to structural vulnerabilities, new parameters could e.g. be the inclusion of economic, ecological, or societal vulnerabilities, as well as indirect impacts. Experience on these issues can probably also be gained from storm surge and coastal flood risk analysis (see e.g. Burzel et al., 2015; Ujeyl and Rose, 2015; for a survey, see NGI, 2014). Also the awareness, education level, and preparedness of the people, as well as existing warning systems and design of mitigation structures influence on exposure and risk, and should be integrated in future analyses. Implementation of breakwaters in the numerical models should consider failure as well as flow through the permeable structure (Cappietti et al., 2012). This could perhaps be achieved by replacing the breakwater by a “high roughness zone” or assign current velocities and surface elevation behind the breakwater of recommended design from the laboratory experiments. Possible examples with inclusion of seawalls/breakwaters should anyhow be presented with caution, as the present structures have a minimal effect on worst-case scenarios like the 2011 Tōhoku tsunami.

Building vulnerability (not treated in this study due to lack of timely available data, but used in previous forecast studies; NGI, 2009c, 2009d) can be assessed quite detailed, in particular when cadastral data are available and combined with ancillary

data such as information on building type from official sources, or from satellite imagery and/or photographs published in GoogleMaps and GoogleEarth. Building fragility curves as presented by among others Suppasri et al. (2011, 2013) and González-Riancho et al. (2014b) should be applied. Refining building vulnerability in this way will allow for a refinement of the mortality risk calculations. Exposure can, for example, be refined by including information about the spatio-temporal whereabouts of people (cf. Freire et al., 2013), or information about the population composition (cf. Maruyama and Tanaka, 2014; González-Riancho et al., 2014b). Fatality-ratio curves by Suppasri et al. (2012) or others should be used to adjust the S-curves used in the computation of the mortality risk. Additionally, the inclusion of evacuation plans (cf. González-Riancho et al., 2013; Bunpei et al., 2015) and shelter locations would help to improve the forecasting capability of the model.

Further experience can be gained e.g. from the HAZUS-MH (Hazards-United States Multi-Hazard) Flood Model (https://www.fema.gov/hazus-multi-hazard-models) that is used to assess both riverine and coastal flooding and estimates potential damage to buildings, essential facilities, transportation lifelines, utility lifelines, vehicles, and agricultural crops. HAZUS-MH also addresses building debris generation and shelter requirements. Direct losses are estimated based on physical damage to structures, contents and building interiors. The effects of flood warning are taken into account, as are flow velocity effects. HAZUS-MH can be run internationally, but without technical support or training for users/analyses outside the U.S. and Canada.

9 Acknowledgements

Prof. T. Arikawa and Prof. Y. Nakamura (PARI) are thanked for providing high resolution digital elevation data which were crucial for the refined tsunami inundation modelling, for guiding us to field survey data on the internet, and for helping out with the translation of these internet pages. We are further truly indebted to Prof. Y. Maruyama for providing the population census data. Prof. J.-D. Schmöcker, Dr. P. González-Riancho Calzada, and Dr. J. Teo are all thanked for helpful advices on additional data to be implemented. This study was supported by funding received from the CONCERT-Japan Joint Call on Efficient Energy Storage and Distribution/Resilience against Disasters (http://www.concertjapan.eu), the Research Council of Norway (contract no. 229578/H20), and the Norwegian Geotechnical Institute.

10 References

Berryman, K. et al. (eds.) (2005): Review of tsunami hazard and risk in New Zealand. Geological and Nuclear Sciences (GNS) report 2005/104. 140 pp.

Bridges, K.-J. 2011. Influence of macro-roughness on tsunami runup & forces. MSc thesis, Oregon State University, http://hdl.handle.net/1957/20794.

Bunpei, N., Shimamoto, H., Nakamura, T., Uno, N., Schmöcker, J.-D., Yamazaki, H. 2015. Evaluation of Tsunami Planning Considering Vehicle Usage and Start Timing of Evacuation. Accepted for presentation at the 6th International Symposium on Transportation Network Reliability (INSTR), August 2015, Nara, Japan.

Burzel, A., Dassanayake, D.R., Oumeraci, H. 2015. Spatial modeling of tangible and intangible losses in integrated coastal flood risk analysis. Coast. Eng. J. 57, DOI: 10.1142/S0578563415400082.

Cappietti, L., Kortenhaus, A., Oumeraci, H. 2012. Laboratory measurements of wave induced mass fluxes at emergent rubble-mound breakwaters. Proceedings of the 4th International Conference on the Application of Physical Modelling to Port and Coastal Protection (Coastlab12), Ghent, Belgium, 217-224.

Dalrymple, R. A., Grilli, S. T., Kirby, J. T. 2006. Tsunamis and challenges for accurate modeling, Advances in Computational Oceanography, 19 (1), 142 -151.

Dominey-Howes, D., Papathoma, M. 2007. Validating the "Papathoma Tsunami Vulnerability Assessment Model" (PTVAM) using field data from the 2004 Indian Ocean tsunami. Natural Hazards 40, 1, 113-136.

Doocy S., Gorokhovich Y., Burnham G., Balk D., Robinson C. 2007. Tsunami Mortality Estimates and Vulnerability Mapping in Aceh, Indonesia. American Journal of Public Health 97 (Suppl. 1):S146-S151. doi:10.2105/AJPH.2006.095240.

Dunbar, P., McCullough, H., Mungov, G., Varner, J., Stroker, K. 2011. 2011 Tohoku earthquake and tsunami data available from the National Oceanic and Atmospheric Administration/National Geophysical Data Center. Geomatics, Natural Hazards and Risk, 2(4), 305-323.

EERI Special Earthquake Report 2011. The Japan Tohoku Tsunami of March 11, 2011, http://www.eqclearinghouse.org/2011-03-11-sendai/files/2011/11/Japan-eq-report-tsunami2.pdf.

Eidsvig, U.M.K., Medina-Cetina, Z., Kveldsvik, V., Glimsdal, S., Harbitz, C.B., Sandersen, F. 2009. Risk assessment of a tsunamigenic rockslide at Åknes. Natural Hazards. DOI 10.1007/s11069-009-9460-6.

EM-DAT 2011. The International Disaster Database: Centre for Research on the Epidemiology of Disasters: http:/www.emdat.be, access date: 13 June.

Freire, S., Aubrecht, C., Wegscheider, S. 2013. Advancing tsunami risk assessment by improving spatio-temporal population exposure and evacuation modeling. Nat Hazards (2013) 68:1311–1324. DOI 10.1007/s11069-013-0603-4

Fraser, S., Leonard, G.S., Matsuo, I., Murakami, H. 2012. Tsunami evacuation: Lessons from the Great East Japan earthquake and tsunami of March 11th 2011, GNS Science Report 2012/17. 89 pp.

GeoSpatial Information Authority of Japan (GSI) 2011. Year 2011 ground due to the Tōhoku Pacific Ocean earthquake subsidence survey. Retrieved July 20, 2011, from http://www.gsi.go.jp/sokuchikijun/sokuchikijun40003.html

Gomez, C., Wassmer, P., Kain, C. L., De Villiers, M., Campbell, K., Ward, S., Moghaddam, A. 2011. GIS Evaluation of the Impacts on the Built and the "Natural Environment of the 11 March 2011 Tsunami in Rikuzentakata, Iwate Prefecture, Japan.

González-Riancho, P., Aguirre-Ayerbe, I., Aniel-Quiroga, I., Abad, S., González, M., Larreynaga, J., Gavidia, F., Gutiérrez, O.Q., Álvarez-Gómez, J.A., Medina, R. 2013. Tsunami evacuation modelling as a tool for risk reduction: application to the coastal area of El Salvador. Nat. Hazards Earth Syst. Sci., 13, 3249–3270. doi:10.5194/nhess-13-3249-2013.

González-Riancho, P., Aguirre-Ayerbe, I., García-Aguilar, O., Medina, R., González, M., Aniel-Quiroga, I., Gutiérrez, O.Q., Álvarez-Gómez, J.A., Larreynaga, J., Gavidia, F. 2014. Integrated tsunami vulnerability and risk assessment: application to the coastal area of El Salvador. Nat. Hazards Earth Syst. Sci., 14, 1123-1244. doi:10.5194/nhess-14-1223-2014a.

González-Riancho, P., Aliaga, B., Hettiarachchi, S., Honzález, M, Medina, R. 2014b. A contribution to the selection of tsunami human vulnerability indicators: conclusions from tsunami impacts in Sri Lanka and Thailand (2004), Samoa (2009), Chile (2010) and Japan (2011). Nat. Hazards Earth Syst. Sci. Discuss., 2, 7679–7734. doi:10.5194/nhessd-2-7679-2014.

Goto, K., Chagué-Goff, C., Fujino, S., Goff, J., Jaffe, B., Nishimura, Y., Richmond, B., Sugawara, D., Szczuciński, W., Tappin, D. R., Witter R. C., Yulianto, E. 2011. New insights of tsunami hazard from the 2011 Tohoku-oki event. Marine Geology, 290, 46-50.

Harbitz, C.B., Sverdrup-Thygeson, K., Kaiser, G., Swarny, R., Gruenburg, L., Glimsdal, S., Løvholt, F., McAdoo, B., Frauenfelder, R. 2009. GIS methodologies for local tsunami risk assessment – validation for the 2009 South Pacific tsunami in American Samoa. EGU Abstract 2011.

Japanese Meteorological Agency 2011. The 2011 off the Pacific coast of Tōhoku Earthquake Portal. Retrieved November 18, 2011, from http://www.jma.go.jp/jma/en/2011_Earthquake.html

Kaiser, G., Scheele, L., Kortenhaus, A., Løvholt, F., Römer, H., Leschka, S. 2011. The influence of land cover roughness on the results of high resolution tsunami inundation modeling. Nat. Hazards Earth Syst. Sci., 11, 2521-2540. doi:10.5194/nhess-11-2521-2011.

Løvholt, F., Kaiser, G., Glimsdal, S., Scheele, L., Harbitz, C.B., Pedersen, G. 2012. Modeling propagation and inundation of the 11 March 2011 Tohoku tsunami. Nat. Hazards Earth Syst. Sci., 12, 1017–1028. doi:10.5194/nhess-12-1017-2012.

Løvholt, F., Setiadi, N.J., Birkmann, J., Harbitz, C.B., Bach, C., Fernando, N., Kaiser, G., Nadim, F. 2014. Tsunami Risk Reduction – Are We Better Prepared Today than in 2004? International Journal of Disaster Risk Reduction 10, 127-142.

Maruyama, Y., Tanaka, H. 2014. Evaluation of Building Damage and Human Casualty after the 2011 off the Pacific Coast of Tohoku Earthquake based on the Population Exposure. Extended Abstract, International Conference on Urban Disaster Reduction - 3ICUDR, Sept. 28.-Oct.1, 2014, Boulder, Colorado, US.

Melgar, L., Lalith, M., Hori, M., Ichimura, T., Tanaka, S. 2014. A Scalable Workbench for Large Urban Area Simulations, Comprised of Resources for Behavioural Models, Interactions and Dynamic Environments. PRIMA 2014: Principles and Practice of Multi-Agent Systems. Lecture Notes in Computer Science Volume 8861, 166-181.

METU 2015. Existing tools, data, and literature on tsunami impact, loads on structures, failure modes and vulnerability assessment. Deliverable D1 of the RAPSODI Project. Norwegian Geotechnical Report 20120768-01-R, 108 pp. http://www.ngi.no/en/Project-pages/RAPSODI/Reports-and-Publications/

Mimura, N., Yasuhara, K., Kawagoe, S., Yokoki, H., Kazama, S. 2011. Damage from the Great East Japan Earthquake and Tsunami – A quick report, Mitig Adapt Strateg Glob Change, doi:10.1007/s11027-011-9297-7.

Mori, N., Takahashi, T., Yasuda, T., Yanagisawa, H. 2011. Survey of 2011 Tohoku earthquake tsunami inundation and run-up, Geophysical Research Letters, 38, L00G14, doi.10.1029/2011GL049210.

Najihah, R., Effendi, D.M., Hairunnisa, M.A., Masiri, K. 2014. Tsunami vulnerability assessment mapping for the west coast of Peninsular Malaysia using a geographical information system (GIS). 8th International Symposium of the Digital Earth (ISDE8), IOP Publishing, IOP Conf. Series: Earth and Environmental Science 18 012047. doi:10.1088/1755-1315/18/1/012047.

NGI 2009a. Local tsunami risk assessment approach: The Bridgetown Demonstration project. Norwegian Geotechnical Institute report 20081430-2. Oslo, Norway.

NGI 2009b. GBV Sårbarhetsanalyser og risikohåndtering – Refined methodology for tsunami risk assessment. Norwegian Geotechnical Institute report 20081430-3. Oslo, Norway.

NGI 2009c. Natural Disaster Mitigation in the Caribbean: Local Tsunami Risk Assessment – The Bridgetown Demonstration Project. Norwegian Geotechnical Institute report 20061575-3. Oslo, Norway.

NGI 2009d. Tsunami Risk Reduction Measures Phase 2: Tsunami risk evaluations for the Philippines. Norwegian Geotechnical Institute report 20061179-00-226-R. Oslo, Norway.

NGI 2011. GBV Sårbarhetsanalyser og risikohåndtering – Analysis of the 2011 Tohoku tsunami. Norwegian Geotechnical Institute report 20081430-00-11-R. Oslo, Norway.

NGI 2014. GBV Storm surge modelling and hazard assessment – Storm surge risk assessment. Norwegian Geotechnical Institute report 20120015-01-R Rev. 1. Oslo, Norway. 162pp.

Ogasawara, T., Matsubayashi, Y., Sakai, S. 2012. Characteristics of the 2011 Tohoku earthquake and tsunami and its impact on the northern Iwate coast, Coastal Engineering Journal, 54 (1), 1250003, 1-16.

Okada, Y. 1985. Surface deformation due to shear and tensile faults in a half-space, Bull. Seism. Soc. Am., 74(4), 1135-1154.

Pedersen, G., Løvholt, F. 2008. Documentation of a global Boussinesq solver. Preprint Series in Applied Mathematics 1, Dept. of Mathematics, University of Oslo, Norway.

Ranghieri, F., Ishiwatari, M. (eds.) 2014. Learning from Megadisasters: Lessons from the Great East Japan Earthquake. Washington DC: World Bank. doi:10.1596/978-1-4648-0153-2. License: Creative Commons Attribution CC BY 3.0 IGO

Sato, M., Ishikawa, T., Ujihara, N., Yoshida, S., Fujita, M., Mochizuki, M., Asada, A. 2011. Displacement above the hypocenter of the 2011 Tōhoku-Oki earthquake. Science (New York, N.Y.), 332(6036), 1395. doi:10.1126/science.1207401.

Sinaga, T.P.T., Nugroho, A., Lee, Y.-W., Suh, Y. 2011. GIS mapping of tsunami vulnerability: Case study of the Jembrana regency in Bali, Indonesia. KSCE Journal of Civil Engineering, Volume 15, Issue 3, 537-543.

Suppasri, A., Koshimura, S., Imamura, F. 2011. Developing tsunami fragility curves based on the satellite remote sensing and the numerical modeling of the 2004 Indian Ocean tsunami in Thailand. Nat Hazards Earth Syst Sci 11, 173–189.

Suppasri, A., Koshimura, S., Imai, K., Mas, E., Gokon, H., Muhari, A., Imamura, F. 2012. Damage characteristic and field survey of the 2011 great east Japan tsunami in Miyagi prefecture, Coastal Engineering Journal, 54 (1), 1250005, 1-30.

Suppasri, A., Mas, E., Charvet, I., Gunasekera, R., Imai, K., Fukutani, Y., Abe, Y., Imamura, F. 2013. Building damage characteristics based on surveyed data and fragility curves of the 2011 Great East Japan tsunami. Nat Hazards 66:319–341. DOI 10.1007/s11069-012-0487-8.

Takahashi, S., Kuriyama, Y., Tomita, T., Kawai, Y. Arikawa, T., Tatsumi, D., Negi, T. 2011. Urgent Survey for 2011 Great East Japan Earthquake and Tsunami

Disaster in Ports and Coasts – Part I (Tsunami). An English Abstract of the Technical Note of Port and Air Port Research Institute, No. 1231, April 28, 2011. http://www.pari.go.jp/en/files/3653/460607839.pdf

Titov, V. V., Moore, C. W., Greenslade, D.J.M., Pattiaratchi, C., Badal, R., Synolakis, C.E., Kânoğlu, U. 2011. A new tool for inundation modeling: Community Modeling Interface for Tsunamis (ComMIT), Pure and Applied Geophysics. doi:10.1007/s00024-011-0292-4.

Tsunami Pilot Study Working Group 2006. Seaside, Oregon tsunami pilot study — modernization of FEMA flood hazard maps. NOAA OAR Special Report, NOAA/OAR/PMEL, Seattle, WA, 94 pp. +7 Appendices.

TU-BS 2015. Results of the laboratory analysis and wave flume tests. Deliverable D7 of the RAPSODI Project. Norwegian Geotechnical Report 20120768-07-R. http://www.ngi.no/en/Project-pages/RAPSODI/Reports-and-Publications/

Ujeyl, G., Rose, J. 2015. Estimating Direct and Indirect Damages from Storm Surges: The Case of Hamburg–Wilhelmsburg. Coast. Eng. J. 57. DOI: 10.1142/S0578563415400069.

Vervaeck, A., Daniell, J. 2011. Japan Tohoku earthquake and tsunami: CATDAT 41 report. http://earthquake-report.com

Review and reference page

Document information		
Document title Deliverable D8 - A GIS tsunami vulnerability and risk assessment model		***Document No.*** 20120768-08-R
Type of document Report	***Distribution*** Limited	***Date*** 30 June 2015 ***Rev. No & date*** 0
Client CONCERT-Japan Joint Call Secretariat		
Keywords		

Geographical information	
Country, County	***Offshore area***
Municipality	***Field name***
Location	***Location***
Map	***Field, Block No.***
UTM-coordinates	

Document control

Quality assurance according to **NS-EN ISO9001**

Rev.	Reason for revision	Self review by:	***Colleague review by:***	***Independent review*** by:	***Inter-disciplinary review by:***
0	Original document	CH			

Document approved for release	**Date**	**Sign. Project Manager**
	30 June 2015	Carl B. Harbitz

CONCERT JAPAN

Connecting and Coordinating
European Research and Technology Development with Japan

concertjapan.eu